Pyörälä *et al. Annals of Forest Science* (2026) 83:9
https://doi.org/10.1186/s13595-026-01326-w

INRAE

Annals of Forest Science

RESEARCH

Open Access

From between-stand to within-tree variation: wood and timber quality of Norway spruce (*Picea abies* H. Karst) analyzed at scale using laser scanning and industrial data

Jiri Pyörälä[1,2*], Mika Pehkonen[2,3], Otto Saikkonen[2], Olli Winberg[1], Xiaowei Yu[1], Johan Holmgren[4], Markus Holopainen[1,2], Juha Hyyppä[1], Harri Kaartinen[1] and Antero Kukko[1]

Abstract

Key message Using laser scanning and industrial data, we found that over 70% of wood quality variability occurred within Norway spruce (*Picea abies* H. Karst) trees. The most important wood quality predictors were stem size, crown vigor, and growth rate inferred from laser scans. Random Forest models based on the laser-scanned features captured 25% of the industrially measured wood quality variability with 39.9% RMSE on average. The low crown plasticity of Norway spruce introduced biological constraints to laser scanning-based wood quality modeling.

Context Wood quality models that also predict wood and timber properties in addition to size and growth variables are essential for increasing the precision of forest management and forest use, yet they remain notoriously untransferable. Laser scanning offers a powerful tool for their parameterization, but its ability to capture the within-tree variability of wood quality is still poorly understood in many species.

Aims Our aim was to test whether multi-viewpoint laser scanning can capture within-tree gradients of wood quality in Norway spruce trees (*Picea abies* H. Karst.), thereby enabling more robust and transferable models.

Methods We analyzed 479 mature Norway spruce trees, combining handheld and airborne laser scanning with industrial wood quality data. We modeled 18 industrially relevant variables related to log geometry, heartwood, knottiness, and timber strength IP value against laser-scanned features at stand, tree, and log levels.

Results Most wood quality variability (73%) occurred within trees. Log-level laser features explained 25% of the variation across stands and log types in the test data, with average RMSEs of 39.9%. The most stable predictions were obtained for heartwood ring width, heartwood density, and knot percentage.

Conclusion Overall, external crown and stem attributes captured key growth responses but failed to robustly represent most wood quality factors in Norway spruce. These results underscore biological constraints in laser scanning-based wood quality modeling depending on the species-specific adaptiveness of the crown structure to the environment.

Keywords Forest management, LiDAR, X-ray tomography, Data fusion, Random forest

Handling editor: Erwin Dreyer.

*Correspondence:
Jiri Pyörälä
jiri.pyorala@helsinki.fi
Full list of author information is available at the end of the article

1 Introduction

Managed forests play crucial roles in climatic and environmental changes. Multiple risks and often contradicting expectations directed at forests introduce difficult trade-offs to their management and use (Achim et al. 2022). Decision-making must consider, e.g., financial return, carbon sequestration potential, product quality, and forest health and resilience (Barrette et al. 2023; Büntgen et al. 2019; Chen et al. 2016; Gauthier et al. 2015; Vauhkonen & Packalen 2018).

Wood properties, such as wood density, and ring and branching properties, affect all aspects of these ecosystem functions and services. Decision-making thus requires robust and flexible model-based tools to estimate the wood properties of standing trees.

Wood properties result from tree growth, i.e., wood formation. Wood formation encompasses primary growth in the apical meristems (shoot elongation, or height growth) and secondary growth induced by the cambium (girth expansion, or radial growth) (Rathgeber et al. 2016). The secondary growth provides trees with their unique capability of growing large and continuing to function, sequester carbon, compete for resources, and acclimate to external changes over decades and centuries. The baseline wood formation functions are driven by intrinsic factors related to tree size and age. These include hydraulic conductance influenced by tree height and crown size and mechanical bearing capacity related to tree mass (Hölttä et al. 2010; Lachenbruch et al. 2011). As a result, often more than half of the wood property variation occurs within individuals (Jyske et al. 2008), rather than between different trees. The environment, climate, silviculture, competition, soil conditions, forest type, and forest health further influence the baseline functions (Barrette et al. 2023; Pretzsch 2021; Zeller & Pretzsch 2019).

The integration of wood properties and quality into growth models and forest simulation frameworks has been extensively studied (Drew et al. 2022; Friend et al. 2019; Mäkelä et al. 2010). Most existing models rely on relatively sparse input variables, such as species or genus, geographic region, forest type or site index, forest or tree height, and diameter, to parameterize functions at the stand or landscape scale.

Remote sensing—and laser scanning in particular—has been explored to provide localized input data and extrapolate such models over broader areas (Babst et al. 2018; Friend et al. 2019; Van Leeuwen et al. 2011). In recent years, many countries and regions have adopted airborne laser scanning (ALS) campaigns with point densities ranging from 5 to over 20 points per square meter. These data enable the segmentation of individual tree crowns, particularly in the upper canopy layers of mature forests.

Tree- and stand-level metrics derived from ALS, such as return intensity and height profiles, canopy openness, and crown size and geometry, correlate with important indicators of wood quality (Pyörälä et al. 2019b) and wood properties (Hilker et al. 2013; Luther et al. 2014; Pokharel et al. 2016). For example, Pokharel et al. (2016) reported that stand-level ALS features explained 39% of the variation in mean wood density in black spruce (*Picea mariana* (Mill.) Britton, Sterns & Poggenb.). Hilker et al. (2013) found that ALS features explained 55–65% of mean wood fiber attributes in lodgepole pine (*Pinus contorta* var. *latifolia* Engelm.), which was 5–10% less accurate than estimates from existing allometric models. Similarly, Luther et al. (2014) explained 18–54% of the variation in select plot-level mean wood properties in black spruce and balsam fir (*Abies balsamea* L.), a level of accuracy comparable to that of large-area models based on stand-level forest inventory variables (Lessard et al. 2014).

Recently, drones and other mobile platforms equipped with lightweight profile scanners have enabled the collection of detailed point clouds both above and beneath forest canopies (Hyyppä et al. 2020a; Wang et al. 2021). Tools for processing such point clouds, such as quantitative structure models (QSMs) implemented in treeQSM (Raumonen et al. 2013), have been extensively applied to data from terrestrial and mobile laser scanning (TLS and MLS, respectively). These methods hold potential for the derivation of wood property and quality indicators (Nocetti & Brunetti 2024) that could depict, in greater detail than ALS, the multiple responses that trees show as they grow, e.g., crown metrics, branching properties, and stem form.

However, Winberg et al. (2023), for example, found that the treeQSM and another method based on density-based spatial clustering of applications with noise (DBSCAN) (Ester et al. 1996) could not fully capture the branching structure of Norway spruce (*Picea abies* (L.) H. Karst.) in MLS data when compared with sawmill-derived internal references. Similar findings regarding the feasibilities of branch extraction methods on MLS and TLS data have been reported by, e.g., Yrttimaa et al. (2023), Hartley et al. (2022), and Pyörälä et al. (2018b).

Nevertheless, the features that can be extracted from TLS and MLS are still sufficient for predicting wood quality, e.g., internal knottiness and wood density (Pyörälä et al. 2019a, 2018a), and even fiber properties such as microfibril angle, coarseness, and fiber length. Côté et al. (2021) reported that TLS-derived fine-scale tree features explained 12–56% of the mean fiber properties at the tree level in black spruce and balsam fir. Giroud et al. (2019) showed that TLS-based stem and crown metrics, when combined with competition and topographic indicators,

explained 33–55% of mean tree-level fiber properties in black spruce. Blanchette et al. (2015) explored the variability of wood properties at an even coarser level: they were able to explain up to 70% of the plot-level mean fiber properties of black spruce and balsam fir with TLS-derived forest metrics.

Nevertheless, the spatial transferability of the laser scanning-based wood quality models has remained rather low, i.e., the most accurate models fitted to one dataset have not performed well in other areas. Recent examples of larger area extrapolation attempts are lacking. Furthermore, the tree- or stand-level mean values for wood properties that are most often considered in the literature still omit significant amounts of the true variability (that occurs within trees). We argue that one potentially crucial factor limiting the accuracy and transferability of wood quality models based on different laser scanning techniques is the lack of accounting for within-tree variability of wood properties and quality. Unfortunately, major practical challenges often hinder the acquisition of sufficiently detailed and extensive wood quality data for modeling at the within-tree level.

Promisingly, laser scanners have been integrated into harvesters (Sagar et al. 2024). Together with continued improvements in drone platforms (Karjalainen et al. 2024), these developments could soon produce vast databases of multi-viewpoint point clouds generated during operational forestry. These forest-acquired point clouds could further be fused with rich data streams collected in industrial wood processing. For example, industrial wood users routinely acquire detailed wood quality information using technologies such as X-rays, sound waves, lasers, and optical systems (Oja et al. 2004). These datasets have so far been rarely integrated with remote sensing data.

In this study, we applied a data-fusion approach that combined above- and below-canopy laser-scanned point clouds with industrial log tomography and timber grading. We focused on Norway spruce, the second main conifer in Fennoscandia alongside Scots pine (*Pinus sylvestris* L.). Whereas Scots pine, with comparatively high crown plasticity, has been more frequently studied and has shown promising results for laser scanning-based wood quality modeling, the potential and limitations for Norway spruce, with a markedly less plastic crown architecture, remain largely unexplored.

We used the Finnish forest type classification as the highest hierarchical level to represent local populations stratified by growth conditions. Forest type is an indicator of site productivity, integrating the effects of soil type, moisture, and fertility, as indicated by ground vegetation. Forest type is generally assumed to influence wood quality through its strong association with site productivity and tree growth rates. Beyond forest type, stand-specific factors, such as thinning intensity, are also considered major drivers of wood quality variation. At the individual tree level, attributes such as tree size and immediate competition via its effects on crown size and structure further contribute to wood property differences.

Our aim was to test a hypothesis that multi-viewpoint point clouds capture key sources of variations in wood properties—from site- and stand-specific factors to within-tree gradients—thereby enabling more robust and transferable wood quality models across spatial scales. Explicitly, our objective was to answer the following research questions: (1) How is the variation in wood properties in Norway spruce hierarchically distributed across spatial levels (forest type, stand, tree, log)? (2) How do wood quality indicators derived from various laser scanning techniques align with these directions of variation? (3) To what extent can wood quality models based on above- and below-canopy laser scanning predict the wood properties of Norway spruce? (4) How robust are these predictions across forest stands?

2 Material and methods

2.1 Study area and materials

The study materials entailed 14 mature Norway spruce-dominated stands from southeastern Finland (Fig. 1). The stands were selected together with the wood buyers of our industrial partner Stora Enso (Stora Enso Metsä oyj, Finland). The stands covered the most common Norway spruce stand conditions within the area (Table 1). Within each stand, we formed 2–5 circular sample plots with a 12-m radius, and within each plot, we selected 6–10 sample trees (Fig. 1). In total, 479 sample trees from 52 sample plots were selected. For each sample tree, the diameter at breast height (*DBH*) and tree height (*H*) were measured using calipers as the mean of two perpendicular measurements, and Vertex IV (Haglöfs AB, Sweden) as the mean of three repeated measurements, respectively.

The stands were clear-cut between October and December 2020. We paint-marked both ends of all sawlogs bucked from the sample trees to trace them to the sawmill (Fig. 1). The stems were bucked to sawlogs with lengths ranging from 4.1 m to 5.7 m at 30-cm intervals. The minimum allowed top diameter was 12 cm. The minimum quality requirement was that each sawlog should stay in one piece after bucking, i.e., anything else was tolerated, including sweep, crook, decay, and ramicorn branches that otherwise downgrade sawlogs to pulp wood. The paint-marked sample tree logs were kept separate from the rest of the logs, hauled to Stora Enso's Honkalahti sawmill in Joutseno (Fig. 1), and stored in a designated pile. One stand experienced harvesting operation delays, and some sample logs were mixed

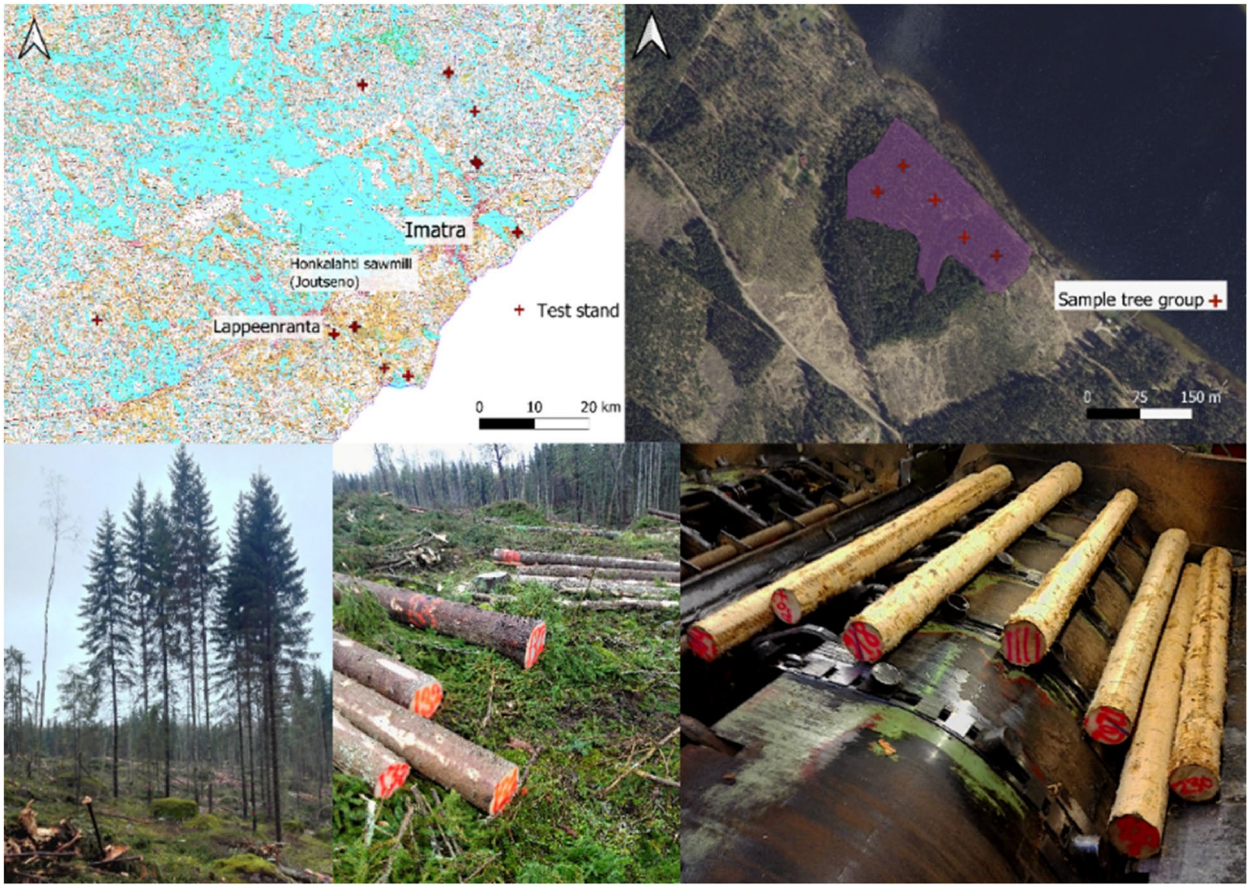

Fig. 1 Study site locations across southeastern Finland, an example of plot locations at one of the studied stands, a sample tree group waiting to be harvested, and examples of tree identification numbers painted on the logs in the forest and at the sawmill

Table 1 Information regarding the analyzed stands. Forest type according to the Finnish classification system (OMT = herb-rich, Oxalis-Myrtillus type, MT/MT + = mesic Myrtillus type, $^{/p}$ denotes stands partly on peatland). *BA* basal area, *Spruce-%* percentage of spruce from the total stand volume, *DBH* mean diameter at breast height, *H* mean tree height

Stand ID	Area, ha	Forest type	BA, m^2/ha	Stems/ha	Volume m^3/ha	Spruce-%	Age, a	DBH, cm	H, m	Sample plots	Sample trees
1	3.3	OMT	25.2	952	389.4	93.5	71	25.3	21	5	42
2	1.8	MT+	31.1	465	273.7	58.7	66	29.8	22	4	31
3	0.8	MT$^{/p}$	23.7	495	188.7	84.1	77	29.1	20	3	22
4	0.6	MT+	31.0	544	274.3	95.2	64	27.4	21	2	17
5	2.8	MT	29.6	600	217.3	66.5	64	26.3	20	4	34
6	3.4	MT+	25.3	524	243.3	85.7	71	27.0	21	5	44
7	1.8	MT+	23.3	407	232.0	86.1	68	29.3	22	4	33
8	2.5	MT$^{/p}$	25.9	482	222.3	59.5	71	27.4	20	5	39
9	2.3	MT	27.3	315	250.0	88.9	90	30.6	26	4	30
10	5.3	MT	33.2	479	417.6	75.6	91	33.2	25	5	46
11	0.9	OMT	32.0	506	274.0	87.1	85	29.0	23	2	18
12	4.7	OMT	25.5	696	226.0	70.1	76	23.7	19	5	44
13	1.6	MT$^{/p}$	30.6	481	344.8	76.2	82	31.2	25	4	33
14	3.8	MT	33.7	632	383.5	77.8	84	28.0	23	5	46

with the bulk of the harvested wood, but 1244 annotated logs eventually found their way to the sawmill within the timeframe scheduled for the measurements. The total fresh volume of the batch was 2945 m^3.

2.2 Airborne laser scanning data

We used an ALS system known as HeliALS-DW that was mounted to a helicopter. The system incorporated a Riegl VUX-1HA scanner (1550 nm) (Riegl GmbH, Austria), Riegl miniVUX-1UAV scanner (905 nm), and a positioning system consisting of a LITEF UIMU-LCI inertial measurement unit (IMU), a NovAtel Flexpak6 GNSS receiver and GGG-703 antenna. The ALS measurements were conducted individually for each test site in October 2020. The flight trajectories consisted of a 2D rectangular grid with flight lines separated by 50 m. The flight speed was 9.5 m/s and the flight altitude approximately 80 m above ground. We used Waypoint Inertial Explorer (version 8.90, NovAtel Inc., Canada) and nine virtual global navigation satellite system (GNSS) base stations from the Trimnet service (RINEX 2.11), situated at each of the test sites and at the airfields, i.e., over an area spanning 40 km in radius, to enable precise georeferencing of the flight trajectories. The raw ALS data were processed using RiProcess software (version 1.8.8, Riegl GmbH, Austria) into point clouds using the obtained trajectory, including further fine-tuning. The final point cloud product was exported in LAS 1.2 format for further processing. Points with reflectance values below − 25 dB or higher than 5 dB were removed from the final point clouds. The reflectance thresholds refer to calibrated reflectance used for quality filtering, but in subsequent data processing we used raw intensity values (at the scale of 0–65,353). The point density of the final VUX-1HA point cloud ranged from 800 pts/m^2 to 6000 pts/m^2 and from 100 pts/m^2 to 600 pts/m^2 in the miniVUX-1UAV point cloud, depending on stand density and structure. For further details on ALS data acquisition and preprocessing, see Hyyppä et al. (2022). Figure 2 presents an example of an ALS point cloud from the stand to tree levels.

2.3 Handheld laser scanning data

All test sites were surveyed by handheld laser scanning (HHLS) using a ZEB Horizon (GeoSLAM, Nottingham, United Kingdom). The survey involved walking through the test stands in a four-leaf clover-shaped pattern with multiple loops passing the sample tree groups. The trajectory was started and ended at the same point to enhance data accuracy. This approach facilitated loop closure detection and minimized drift and offset errors in the

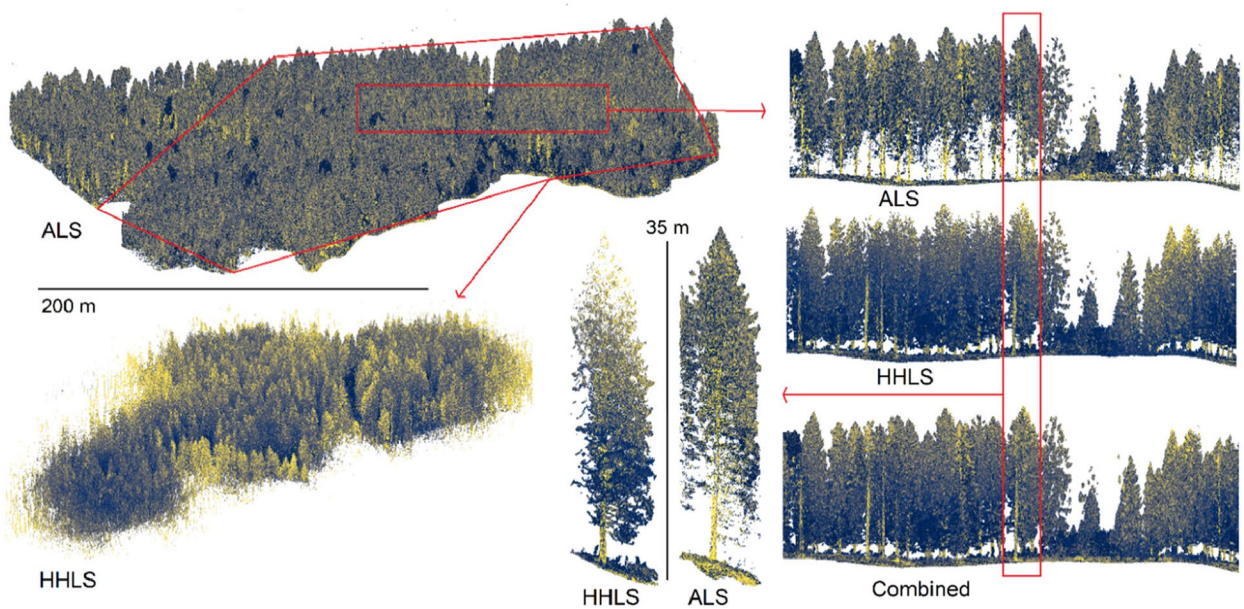

Fig. 2 Example of point clouds from handheld and airborne laser scanning (HHLS and ALS, respectively). The ALS data were VUX-1HA data measured from a helicopter (point densities 800–6000 pts/m^2) and cover entire stands wall-to-wall. The HHLS data were collected from a trajectory connecting the sample tree groups, entailing loop closure at several points along the trajectory and at its end. Due to the high density of the ALS data, it depicts the Norway spruce crowns in detail and even some returns from the tree stems. The HHLS data depicts the stems and the lower parts of the crowns in greater detail, but some occlusion is inevitable towards the crowns. The colors represent the raw intensity of the laser returns (scaled from 0 to 65,535). Brighter yellow tones indicate higher return intensity. The HHLS data generally show lower intensities due to lower pulse energy, and the later ALS returns that penetrate deeper into the canopy also exhibit reduced intensity. Consequently, the lower parts of the trees appear in darker shades

point clouds (Hyyppä et al. (2020b), see Fig. 4c of their work). The walking speed was approximately 2 km/h, and the scanner was held upright at a fixed height of 1.2 m above the ground. Each stand took approximately 20 min to record.

Following data collection, the raw data underwent preprocessing in the GeoSLAM Hub software (version 6.0.0.). Default processing parameters were utilized, including "Convergence threshold": 0, "Window size": 0, "Voxel density": 1, "Rigidity": 0, "Maximum range": 100 m, and "Closed Loop". Subsequently, the processed point cloud data were exported in LAS format for further analysis. The quality of the scans was verified, similarly to Hyyppä et al. (2022). Figure 2 presents an example of an HHLS point cloud from the stand to tree levels, combined with ALS.

2.4 Sawmill data

At the sawmill, the logs were X-rayed using a two-directional FUSION G3X digital radiographer (Finnos oy, Lappeenranta, Finland) with 0.7-mm effective resolution. From the X-ray measurements, over 100 features were calculated for each log using the in-house algorithms from Finnos. We targeted 11 variables in our model analyses:

- Log geometry (4): log volume, taper, sweep, and crook.
- Knottiness (4): number of whorls within log, mean distance between the whorls, knot percentage (knot-to-stem volume ratio), and mean whorl volume.
- Heartwood properties (3): mean ring width, heartwood volume, and mean heartwood density.

In addition, we gathered the X-ray-measured top-end diameters (D_{topX}) and log lengths (L), used them and the Tree IDs to infer log top end heights (i.e., height from the ground; H_{top}), and considered these four as explanatory features in our models (see Table 2 and chapter *Statistical analysis*).

A subsample of 728 logs was sorted into three sawing assortments (I–III) based on the D_{topX}. From each of these logs, two core battens of 50×150 mm or 47×148 mm in cross-sectional dimension were sawn, depending on the top end diameter of the log: I) D_{topX} 270–300 mm to 50×150 mm core battens, II) D_{topX} 210–240 mm to 50×150 mm core battens, and III) D_{topX} 170–200 mm to 47×148 mm core battens. All faces and edges of each fresh sawn piece of wood were analyzed with a FinScan BoardMaster NT (MiCROTEC Srl, Bressanone, Italy) imaging device, and several hundreds of features were calculated. We targeted the following seven timber-grading features on the sawn core timber battens:

- Knottiness (6): statistics of dry and fresh knots (numbers and mean and maximum diameters) (averaged from both faces of the battens).
- Timber strength (1): strength IP value, i.e., an indicator of the modulus of rupture of the batten based on the number, size, and distribution of the knots, in accordance with the Scandinavian timber grading standard INSTA-142 (compatible with the European standard EN-14081-1). N.B.: While IP correlates with

Table 2 The explanatory variables used in this study, grouped by the respective feature space. *NOF* number of features, *DBH* diameter at breast height, *H* tree height, H_{top} and H_{butt} height of the sawlog top and butt, *L* sawlog length, D_{topX} and D_{buttX} diameter of the sawlog top and butt from the X-ray, *LAD* leaf area density, *CGF* canopy gap fraction, *VM05* 0.5-m voxel metrics, *CPA* crown projection area, *CrVol* crown volume, *CrVolUp* crown volume above 50-% height, *relCrVol CrVolUp/CrVol*, *RI* rumple index, *VCI* vertical complexity index, *zq* height quantile, *pzabovezmean* percentage of points above mean height, *pnth* percentage of n^{th} returns, *Zpcum* percentage of points cumulated up to the given height, *NIR1-i* and *NIR2-i*: return intensities of near-infrared 905 nm and 1550 nm wavelengths, respectively, *NDI* normalized difference index between the NIR1 and NIR2 wavelengths, D_{topH} and D_{buttH} diameter of the sawlog top and butt derived from HHLS, *LogVol* log volume, *FF* form factor of the log, *Taper* taper of the log, *relTaper* D_{topH}/D_{buttH}, *KnotVol* total knot volume, *KnotVolmean* mean knot volume of whorls, *KnotVolmax* maximum knot volume of whorls, *KI* knot index, N_{whorls} number of branch whorls, D_{branch} branch diameter, A_{branch} branch insertion angle, $Dist_{whorls}$ distance between whorls

Feature space	Features	NOF
1 Stand	Stand volume/ha, stems/ha, pine-% (of m^3), broadleaved-% (of m^3), spruce mean *DBH*, spruce mean *H*, spruce stems/ha, forest type	8
2 Tree	*H*, *DBH*, $H/maxH_{plot}$, $H/meanH_{plot}$, $DBH/maxDBH_{plot}$, $DBH/meanDBH_{plot}$	6
3 Log	H_{top}, *L*, D_{topX}, D_{buttX}	4
4 ALS (geometric)	max, mean, sd, skew., and kurt. of *Z*, *LAD*, *CGF*, *VM05*, *CPA*, and *CrVol*, *CrVolUp*, *relCrVol*, *RI*, *VCI*, *zq90*, *zq95*, *pzabovemean*, *p2th*, *Zpcum5*, *Zpcum9*	32
5 ALS (spectral)	max, mean, sd, skew., and kurt. of i_{NIR1} and i_{NIR2}, ratios i_{NIR1}/i_{NIR2}, and *NDI*; all, 1 st returns, 2nd returns and late returns separately + *p1th* and *p2th* for NIR1 and NIR2 separately and together	48
6 HHLS	D_{topH}, D_{buttH}, *LogVol*, *FF*, *Taper*, *relTaper*, *KnotVol*, *KnotVolmean*, *KnotVolmax*, *KI*, *Nwhorls*, max, mean, min, sd, skew., and kurt. of D_{branch}, A_{branch}, *DistWhorls*	29

the modulus of rupture (typically $R^2 = 0.6–0.7$; see, e.g., Hanhijärvi et al. (2005)), it is an indirect indicator and not a direct measurement of actual bending strength. Accordingly, we report results as associations with the IP value rather than as true timber strength.

Placement of the logs in both the X-raying device and the sawing were videoed, and we read the Tree IDs from the log ends on the videos to link the X-ray and timber-grading data to respective sample trees (see chapter *Data fusion*). We successfully identified 1130 X-rayed logs from 450 trees and 604 sawn logs from 365 trees.

In this study, we used the sawmill data as a reference standard at the operational level, consistent with their intended industrial purpose, similarly to, e.g., Pyörälä et al. (2018a and 2019a). The features used in this study are the same variables employed in industrial log and timber grading. Their measurement accuracy is considered sufficient for operational decisions, including but not limited to sorting timber for structural use (strength grading), identifying wood suitable for lamella production (based on knot cluster spacing), and selecting material for carpentry (e.g., absence of large dead knots or suitable ring width). For example, Oja et al. (2003) showed that the grading accuracy of sawlogs was 77–83% with a similar device.

Based on available documentation, the FUSION G3X applies a single-energy, dual-view X-ray configuration optimized for high-throughput log sorting. Similar industrial X-ray scanners have been widely evaluated in the literature and shown to provide repeatable and sufficiently accurate estimates of wood properties for operational use at industrial sawmills (Oja et al. 2004; Sandberg et al. 2023; Wei et al. 2011).

The wood density values provided by the FUSION G3X system were directly derived from X-ray attenuation at the 0.7-mm pixel level, which follows well-established physical relationships with wood density in moist material (Liu et al. 1988; Olson et al. 1988). Literature shows that green wood density can be measured with mean errors between 1 and 15 kg/m^3, depending on species, wood moisture, and scanning configuration (Wei et al. 2011). The density values were averaged over the entire log to represent apparent green density (green weight over green volume), as used in operational log sorting. The measurement routine was identical to what is operationally used, and we therefore assume that the logs passed through the scanner under their typical operational moisture conditions and that the scanner's internal calibration sufficiently compensated for moisture variability for industrial use. However, to be careful not to overinterpret the results, we considered the wood density estimates consistent across the studied stands and logs scanned under similar operational conditions and avoided direct comparisons of the absolute density values per se with the existing literature.

The delineation of internal quality features in heartwood, i.e., knot clusters (whorls), rings, and heartwood boundary was based on detecting the sharp boundaries in wood density values, e.g., between stemwood and knot wood, latewood and earlywood, and sapwood and heartwood (Johansson et al. 2013; Longuetaud et al. 2007). The delineation used a combination of deep-learning edge-detection and template matching techniques trained by Finnos. Similar approaches have shown good agreement with reference values, e.g., a 1.8-mm mean error in heartwood and sapwood separation (Longuetaud et al. 2007) and 88–94% knot detection accuracy (Johansson et al. 2013). We concentrated on heartwood-derived variables, where the influence of moisture variability on X-ray attenuation is smaller than in sapwood.

2.5 Segmentation and extraction of features from the ALS point clouds

The aims of this study, which concentrated on identifying the relevance of various spatial levels on wood quality from the forest type and stand level to the individual tree level, required identification and extraction of individual trees from the point cloud data. In ALS data, this procedure refers to individual tree delineation, which entails the segmentation of the canopy layer into individual tree crowns that are henceforth called crown segments. Here, we delineated the crown segments from the point clouds and calculated tree-specific features for each crown segment using the lidR package (Roussel & Auty 2024; Roussel et al. 2020) in R software (R, 2023). Ground points were classified, and the point heights were normalized with respect to the ground points. The crown segmentation was done on the height-normalized canopy height model using a local-maxima filter with a moving 4-m circular window to detect treetops and a watershed algorithm-based method to delineate the crowns using treetops as seed positions (Dalponte & Coomes 2016). For each delineated crown segment, 37 geometrical features were calculated (Table 2):

- The heights where 90% and 95% of points had accumulated (*zq90* and *zq95*, respectively, depicting tree height).
- The crown volume as an alpha shape fitted to the first returns in the segment (*CrVol*, with an alpha value of 10 m, see Edelsbrunner and Mücke (1994)) to represent crown size.

- The crown volume above 50% height (*CrVolUp*) and its relative value (*relCrVol* = *CrVolUp*/*CrVol*) as a descriptor of crown shape.
- The crown surface area (*CrA*), as a feature for crown size.
- Percentage of points above the mean height (*pzabovezmean*), descriptive of crown shape and openness.
- The rumple index, *RI*, the roughness of a surface as the ratio between its area and its projected area on the ground: descriptive of crown shape and evenness (Jenness 2004).
- The vertical complexity index (*VCI*, a fixed normalization of the entropy function (van Ewijk et al. 2011), to depict the evenness (and length) of the crown).
- The percentage of points accumulated at 5 and 9 m above ground (*Zpcum5* and *Zpcum9*), depicting crown length and canopy openness.
- The percentage of 1 st and 2nd returns of all returns (*p1th*, *p2th*), to represent crown shape and canopy openness.
- The mean, maximum, standard deviation, skewness, and kurtosis of:
    - Normalized point heights (*Zmean*, *Zmax*, *Zsd*, *Zskew*, *Zkurt*, respectively),
    - Leaf area density profiles (*LADmean*, *LADmax*, *LADsd*, *LADskew*, *LADkurt*),
    - Canopy gap fraction profiles (*CGFmean*, *CGFmax*, *CGFsd*, *CGFskew*, *CGFkurt*),
    - Crown projection area profiles (*CPAmean*, *CPAmax*, *CPAsd*, *CPAskew*, *CPAkurt*), and
    - 0.5-m voxel metric profiles (*VM05mean*, *VM05max*, *VM05sd*, *VM05skew*, *VM05kurt*)

The vertical profiles of canopy gap fraction, leaf density area, crown projection area, and voxel metrics were based on values observed from vertical slices of 1 m in height. They were assumed to represent the shape of the tree crowns and were thus characteristically different across forest types or competitive situations. The canopy gap fraction was estimated as the ratio between returns within and below the targeted slice and the total number of returns, and the leaf-area density was defined as the natural logarithm of the canopy gap fraction, divided by an extinction coefficient $k = 0.5$ (Bouvier et al. 2015). The crown projection area was the convex hull-based estimate of the area occupied by points, and the voxel metrics were the number of 0.5-m voxels occupied by points in each slice. Moreover, 48 spectral features were derived, describing the distribution and statistics of the intensities (i) from the two near-infrared wavelengths (NIR1: 905 nm and NIR2: 1550 nm) (Table 2). We calculated mean, maximum, standard deviation, skewness, and kurtosis of i for both wavelengths, the ratios between the mean and standard deviation values of both wavelengths and the normalized difference index *NDI* as i_{NIR1}-i_{NIR2}/i_{NIR1} + i_{NIR2} separately for the different return groups and using all returns. The spectral features were considered representative of crown vigor, i.e., the combined effects of health, water content, and foliage density.

Finally, we calculated the geometrical and spectral ALS features also for vertical sections of the crown segments that corresponded to the sawlog heights in the sawmill data (see chapter *Data fusion*). Segmenting crowns vertically was expected to reveal finer structural differences relevant to log-level quality—for example, distinguishing butt logs from trees with similar overall height and crown width but differing crown positions, which could result in different crown influence at the butt-log height. See Table 2 for an exhaustive list of all features.

2.6 Reconstruction of tree stems and branching from HHLS point clouds

We processed the HHLS point clouds by filtering out spatial outliers based on local neighborhood densities and extracted individual tree stems from the point clouds. The method pipeline consisted of arc detection, random sample consensus (RANSAC) circle fitting (Fischler & Bolles 1981), and classification of point orientation and flatness, following the procedure in Hyyppä et al. (2020b). Stem geometry features were derived using existing stem taper models reparameterized based on the HHLS-derived stem curve measurements: The stem diameter observations were expressed relative to the stem diameter at 20% height, divided into height bins corresponding to 5% height intervals, and the stem taper model from Laasasenaho (1982) was reparameterized according to the relative diameters (see Saikkonen et al. (n.d.) (In review) for details). With the refitted stem taper functions, we calculated the following features for each log: diameters of the log top and butt end from HHLS (D_{topH} and D_{buttH}, respectively), log volume (*LogVol*) log taper (*Taper*) as $(D_{buttH} - D_{topH})/L$ (log length), relative log taper (*relTaper*) as D_{topH}/D_{buttH}, and log form factor (*FF*) as $LogVol/\pi(D_{buttH}/2)^2$.

After tree stem extraction, the point clouds were segmented into individual-tree-level point clouds, and the points around the tree stems (within a 1-m radius) were subjected to the extraction of the branching structures using the quantitative structure model algorithm (treeQSM, (Raumonen et al. 2013) with the approach described in Winberg et al. (2023). Using the branches extracted from the HHLS point clouds, we calculated the number of whorls and the minimum, mean, maximum, standard deviation, skewness, and kurtosis of branch

diameters (D_{branch}), branch insertion angles (A_{branch}), and whorl-to-whorl distances (*DistWhorls*). Branch insertion angles were defined based on the eigenvector direction of the branch points, and branch diameters were estimated by RANSAC circle fitting on branch points projected perpendicular to the branch eigenvector. Branch whorls were separated by hierarchical clustering using a 0.1-m distance threshold. In addition, we calculated direct proxies of the X-rayed variables total, mean, and maximum whorl-level knot volumes (*KnotVol, KnotVolmean, KnotVolmax*), knot percentage (or knot index, *KI*) as *KnotVol/LogVol*, and the number of whorls (*Nwhorls*) within each log (see Winberg et al. (2023) for details).

2.7 Data fusion

The data produced from HHLS and ALS were linked at the tree level by matching the tree maps generated from each data source. We used the matching methods from Hyyppä et al. (2020a), accompanied by manual verification and adjustments of the matching results. We used the matched tree maps to link the ALS crown segments with the Tree IDs known from the paper sheet identified in the HHLS point clouds. The annotated tree-level laser-scanned data were linked, based on the Tree IDs, to respective sawmill references, separately for the X-rayed variables, and the timber grading variables, based on Tree IDs read from the log ends in the video of feeding the logs into X-raying and sawing. The fused datasets and their respective sample sizes used in the statistical analyses are presented in Table 3. Figure 3 illustrates examples of tree-level fused ALS-HHLS point clouds and sawmill data grouped by forest type.

2.8 Statistical analysis

To address the first and second research questions, we used linear mixed-effect models (LMEM) (Pinheiro & Bates 2009). With LMEMs, we analyzed the level of variance in wood and timber quality and the laser-scanned features associated with forest type, and stand-, tree-, and log-level factors. We first observed the variance of tree-level intercepts in the LMEMs nested within stands nested within the forest type strata. The variance explained by the hierarchically nested random parts was compared to the residual variance (unexplained, i.e., due to the log-level variance) of the models to infer the level of variance associated with each of the four levels.

To answer the third and fourth research questions, we used the Random Forest algorithm (RF) (Breiman 2001). RF is a machine learning method that builds multiple regression trees on random subsets of the data and averages their predictions. This approach improves prediction accuracy, reduces overfitting, and allows assessing variable importance through the impact of each predictor on the model's out-of-bag (OOB) error. We chose RF as an example of a machine learning-based approach to perform efficient feature selection from a large set of parallel explanatory features. RF is widely used in forestry-related studies because it can handle high-dimensional, correlated features, automatically assess feature importance, and capture nonlinear relationships without requiring prior assumptions about data distributions. Using RF, we (i) analyzed the level of variance in wood and timber quality explained by the hierarchical levels and data sources, (ii) identified the most important factors, and (iii) assessed the model performance and transferability in predicting wood quality. Nine feature spaces of predictor variables were used (see list of variables in Table 2):

1. Stand-level forest inventory variables,
2. Tree-level field variables,
3. Log-level sawmill measurements (dimensions and height),
4. Tree-level geometrical ALS features,
5. Log-level geometrical ALS features,
6. Tree-level spectral ALS features,
7. Log-level spectral ALS features,
8. Log-level HHLS branching and stem features, and
9. Combined log-level HHLS and tree-level ALS features.

To account for the randomness of the RF predictions, each model was fitted 100 times, each time using different training data and test data from randomly divided data in an 80/20 ratio, respectively. The pre-selection of the explanatory variables to each RF model was based on the ten most important features of a single regression tree fitted to the training data in each case (Pyörälä et al. 2019b). Subsequently, the RF models trained using the ten preselected features consisted of 1999 regression trees, with a minimum node size of 10, and two variables permuted in each node.

Table 3 The sizes of fused datasets between the predictor (laser scans or sawmill/field data) and target feature spaces (X-ray and timber-grading variables)

Predictors	Targets	Stands	Trees	Logs
Sawmill/field	X-ray	14	450	1130
	Timber	14	365	604
HHLS	X-ray	13	330	833
	Timber	13	274	455
ALS	X-ray	11	263	488
	Timber	11	160	222
HHLS+ ALS	X-ray	10	258	657
	Timber	10	212	354

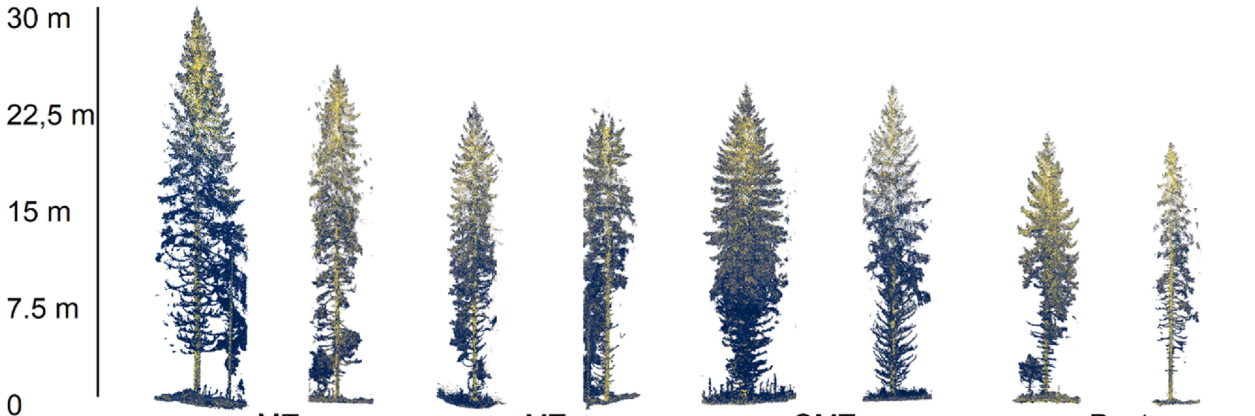

	MT		MT+		OMT		Peat	
H	30.7 m	26.5 m	23.4 m	22.9 m	25.5 m	25.4 m	20.8 m	21.0 m
DBH	41.6 cm	30.0 cm	28.8 cm	25.6 cm	34.5 cm	29.5 cm	26.1 cm	28.7 cm
Ring width	3.7 mm	1.8 mm	3.5 mm	3.1 mm	4.5 mm	3.8 mm	3.1 mm	2.3 mm
Wood density	452 kg/m³	571 kg/m³	416 kg/m³	571 kg/m³	470 kg/m³	517 kg/m³	439 kg/m³	536.5 kg/m³
Strength	48.3	46.5	47.4	48.8	45.3	44.9	45.3	47.1
Mean br. diam.	5.1 cm	4.4 cm	5.1 cm	5.1 cm	6.4 cm	6.2 cm	6.2 cm	4.9 cm
VCI	0.70	0.63	0.61	0.74	0.60	0.76	0.59	0.51
NDI	-0.01	0.01	-0.04	-0.05	0.01	0.08	-0.02	-0.05

Fig. 3 Examples of the studied trees to exemplify how the dependencies between tree characteristics and wood and timber properties may vary between forest types. Two example trees were selected from different forest types (according to the Finnish system: OMT = herb-rich, Oxalis-Myrtillus type, MT/MT+ = mesic Myrtillus type). The point clouds entail combined handheld laser-scanned point clouds and the aerial laser-scanned point clouds (see Fig. 2 for comparison of these point cloud types). Key tree, wood, and timber property variables are reported for the example trees. VCI = vertical complexity index, NDI = normalized difference index. The colors represent the raw intensity of the laser returns (scaled from 0 to 65,535). Brighter yellow tones indicate higher return intensity. The HHLS data generally show lower intensities due to lower pulse energy, and the later ALS returns that penetrate deeper into the canopy also exhibit reduced intensity. Consequently, the lower parts of the trees appear in darker shades

We evaluated the prediction accuracies against the values observed in the sawmill data using the coefficient of determination (R^2), and the root-mean-squared error relative to the mean of the references (RMSE-%) and reported their averages across the 100 rounds. The RMSE-% was found useful, as it provides a scale-normalized expression of RMSE and enables comparable error interpretations across variables with different units. R^2s and RMSE-%s were assessed separately for the training data (to assess the level of variance associated with each hierarchical level) and test data (to assess model robustness and transferability). The most important predictors were identified as those causing the largest increase in OOB MSE when permuted. We reported the five most important factors for each wood quality variable that appeared most frequently in the top five most important factors in each 100 fits.

3 Results

3.1 Wood quality variability associated with forest type and the stand, tree, and log levels

3.1.1 Overview

LMEMs showed that 73% of the wood quality variance occurred within trees, i.e., depending on log height or type (from butt logs to top logs): the log-level residual variance in the LMEMs was 64% for the X-rayed features and 92% for the sawn timber variables, after accounting for forest type and stand- and tree-level random variances (Table 4). The differences between trees accounted for 23% and 6% of the variances in the X-ray and sawn timber grading, respectively, while stand and forest type explained only a minor portion of the variance (Table 4). In alignment with the wood quality variables, the predictor features extracted from HHLS and ALS showed the most variance within trees (Table 4). However, there were some exceptions, where larger proportions of the variances originated higher in the hierarchy, e.g., heartwood ring width (forest type: 22%, stand level: 32%), mean whorl distance (tree level: 36%), and sweep and crook (tree level: 24% and 28%, respectively) (Table 5).

3.1.2 Log geometry

Log volumes were consistent between the log types across all forest types (Fig. 4a), as well as the absolute taper values that increased towards the top logs (Fig. 4b). Relative log taper values measured from the HHLS data showed more distinctive values for peatland

Table 4 The proportion of variance associated with hierarchical levels in different features spaces (mean, and standard deviation, sd): X-rayed wood quality variables, sawn timber variables, geometrical and spectral features from airborne-laser scanning (ALS), and stem and branching features from handheld laser scanning (HHLS)

Feature space	Level of hierarchy	Mean (%-unit)	sd (%-unit)
X-ray	Forest type	3.8	4.1
	Stand	9.2	12.1
	Tree	22.7	11.1
	Log	64.3	20.2
Timber grading	Forest type	0.5	0.6
	Stand	1.3	1.2
	Tree	6.3	8.2
	Log	92.0	7.7
ALS geom	Forest type	1.3	1.8
	Stand	1.7	2.4
	Tree	4.0	7.6
	Log	93.1	10.0
ALS spectr	Forest type	1.2	2.3
	Stand	9.1	8.9
	Tree	10.4	9.0
	Log	79.4	13.9
HHLS	Forest type	0.9	1.3
	Stand	8.4	9.2
	Tree	21.3	12.6
	Log	69.5	16.4

top logs that displayed the smallest relative values (i.e., exhibited the most conical stem shapes) (Fig. 4j). Sweep was generally largest in butt logs, especially in the OMT stands (Fig. 4c).

3.1.3 Knottiness

Knot percentage increased in the uppermost logs, and the highest values were observed in the MT+stands (Fig. 4d). However, the largest mean branch diameters were recorded with HHLS in butt logs from OMT stands (Fig. 4l). The largest branches were most likely dead branches, since the highest frequencies of dead knots were also found in the butt logs, especially in OMT and peatlands (Fig. 4h). Fresh knot diameters increased towards the top logs, with the largest ones on peatlands (Fig. 4g). No major differences were found in HHLS-recorded mean whorl-to-whorl distances between forest types, but slightly higher values were observed in MT top logs and peatland butt logs (Fig. 4k).

3.1.4 Heartwood properties

Heartwood ring width was largest in the more fertile MT+and OMT stands (Fig. 4e), which was accompanied by a slightly lower heartwood density in the OMT stands (Fig. 4f). However, both ring width and wood density within trees increased from the butt logs to top logs—except for ring width in OMT that was equally large across all log types. Core timber strength IP value did not differ remarkably between the forest or log types, except for the notably lower values in the peatland top logs (Fig. 4i).

3.1.5 Crown properties

The ALS-based crown projection area increased from butt logs to top logs, and the widest crowns were found on peatlands (Fig. 4m). *VCI* and *NDI* of the crowns decreased from the bottom to the top (Fig. 4n,), indicating the presence of live foliage and that the point clouds were more densely and uniformly populated within the live crown. However, it is also possible that *VCI* and *NDI* simply increased towards the lower parts of the crowns due to fewer and more attenuated signal returns.

3.2 Analysis of the wood quality models based on above- and below-canopy laser scanning

3.2.1 Overview

According to RF, the most important wood quality predictors across all the hierarchical levels were related to tree size, growth rate, and within-tree position: mean height of the spruce trees, stand volume, and forest type at the stand level; DBH and tree-level crown volume; and log dimensions, log taper and volume, along log-level branch diameters (Table 6). With the ALS data, *NDI* and statistics related to the return intensities of the two wavelengths (which may be interpreted as signals of crown vigor) were among the most common explanators of several wood quality variables at both the tree and log levels (Table 6).

In the training data, log-level features explained over 90% of the wood quality variability in RF (average RMSE=15.5–16.7% across all features), while tree-level variables explained, on average, 64% of the variability with 27–28 RMSE-%s (Table 8, in the Appendix). Stand-level features accounted for 11% of the variabilities on average, with an RMSE=42.2% for the training data (Table 8, in the Appendix). Regardless of the data source in RF, the different feature spaces depicting the same level of hierarchy explained similar levels of variability in the training data (Table 8, in the Appendix).

3.2.2 Log geometry

HHLS-derived log butt diameter and relative taper were the main predictors of log volume and log taper, respectively (Table 6). In butt logs, a larger log volume was associated with smaller relative taper values, i.e., a more conical shape (Fig. 5b1). In middle and top logs, relative

Table 5 The variance level (%) explained by the hierarchical levels for wood quality variables according to the linear mixed effects models. Color coding is row specific, indicating the variance level explained (smallest variance = dark red, largest variance = dark green)

		X-ray										Timber grading									
		Geometry				Heartwood				Knottiness					Knottiness						Mean
		Log volume	Taper	Sweep	Crook	Heartwood volume	Heartwood density	Heartwood ring width	Knot whorls	Mean whorl distance	Knot percentage	Mean whorl volume	Dead knots	Dead knot max d	Dead knot mean d	Fresh knots	Fresh knot max d	Fresh knot mean d	Strength IP value	
	Forest type	1.8	0.0	5.7	5.2	5.4	7.4	21.8	2.1	0.0	1.3	2.2	0.0	0.0	0.0	0.0	0.0	2.1	0.0	**3.1**
	Stand level	3.6	1.5	0.0	2.7	5.6	12.8	31.6	8.0	11.1	5.9	1.8	13.5	1.7	2.9	14.1	0.5	1.7	1.4	**6.7**
	Tree level	23.2	0.0	24.1	28.3	19.7	22.4	24.6	21.2	35.5	21.6	3.5	9.8	0.0	0.0	24.7	26.1	19.9	9.8	**17.5**
	Log level	71.4	98.5	70.3	63.8	69.4	57.4	22.0	68.7	53.5	71.3	92.5	76.6	98.3	97.1	61.2	73.4	76.3	88.8	**72.8**

log taper value increased with higher log volume, indicating a more cylindrical shape (Fig. 5b1).

Crown volume, *Zmean*, and *NDI* were the main log volume predictors in ALS (Table 6). Larger crown areas measured from the ALS data naturally increased with log volumes (Fig. 5d1). *VCI* generally increased with log size, except in the top logs (Fig. 5e1). Moreover, higher *NDI* was associated with greater log volume in most groups, except butt logs from MT+ and OMT stands (Fig. 5f1).

Maximum and mean branch diameter measured from the HHLS data and tree height (*Zmax*) and crown area measured from the ALS data were key predictors of log-level sweep and crook in the RF models (Table 6). Interestingly, tree-level *VCI* was also a good indicator of sweep. In line with this, larger branch diameters, shorter whorl distances, and larger crown areas aligned with more severe sweep (Fig. 5a2, c2, d2).

3.2.3 Knottiness

HHLS-derived log size (D_{buttH}) and ALS-derived *Zmax* and *NDI* were the main indicators for the number of whorls and mean whorl distances at the log level (Table 6). However, knot percentage was best predicted by relative log taper from HHLS (Table 6): more conical logs displayed larger knot percentages (Fig. 5b3).

Larger branch diameters from HHLS indicated a higher knot percentage in butt logs and MT+top logs but a lower percentage in the other groups (Fig. 5a3). It is noteworthy that the HHLS-derived mean branch diameter exhibited log type-dependent relationships with log volume (Fig. 5a1): it increased with log volume in butt logs but decreased in the middle and top logs.

Longer whorl distances generally indicated smaller knot percentages, except in the top logs from MT+and peatland sites (Fig. 5c3). Mean whorl-to-whorl distances slightly decreased with increasing log volume (Fig. 5c1).

The relationship between *NDI* and knot percentage was positive in top logs (except for MT+) and negative in butt logs (Fig. 5f3).

HHLS-derived relative log taper and mean branch diameter were the best predictors of core timber fresh knot size (Table 6). The mean fresh knot diameter generally increased with HHLS branch diameter, except for peatland top logs. However, the correlations of whorl-to-whorl distance with fresh knot size in the core timber were less obvious (Fig. 5c6).

ALS-derived crown volume (both at the tree and log levels) was also an important predictor of core timber fresh knot size (Table 6). In alignment, crown projection area measured from the ALS data correlated positively with the fresh knot diameters, especially in the top logs and butt logs (Fig. 5d6).

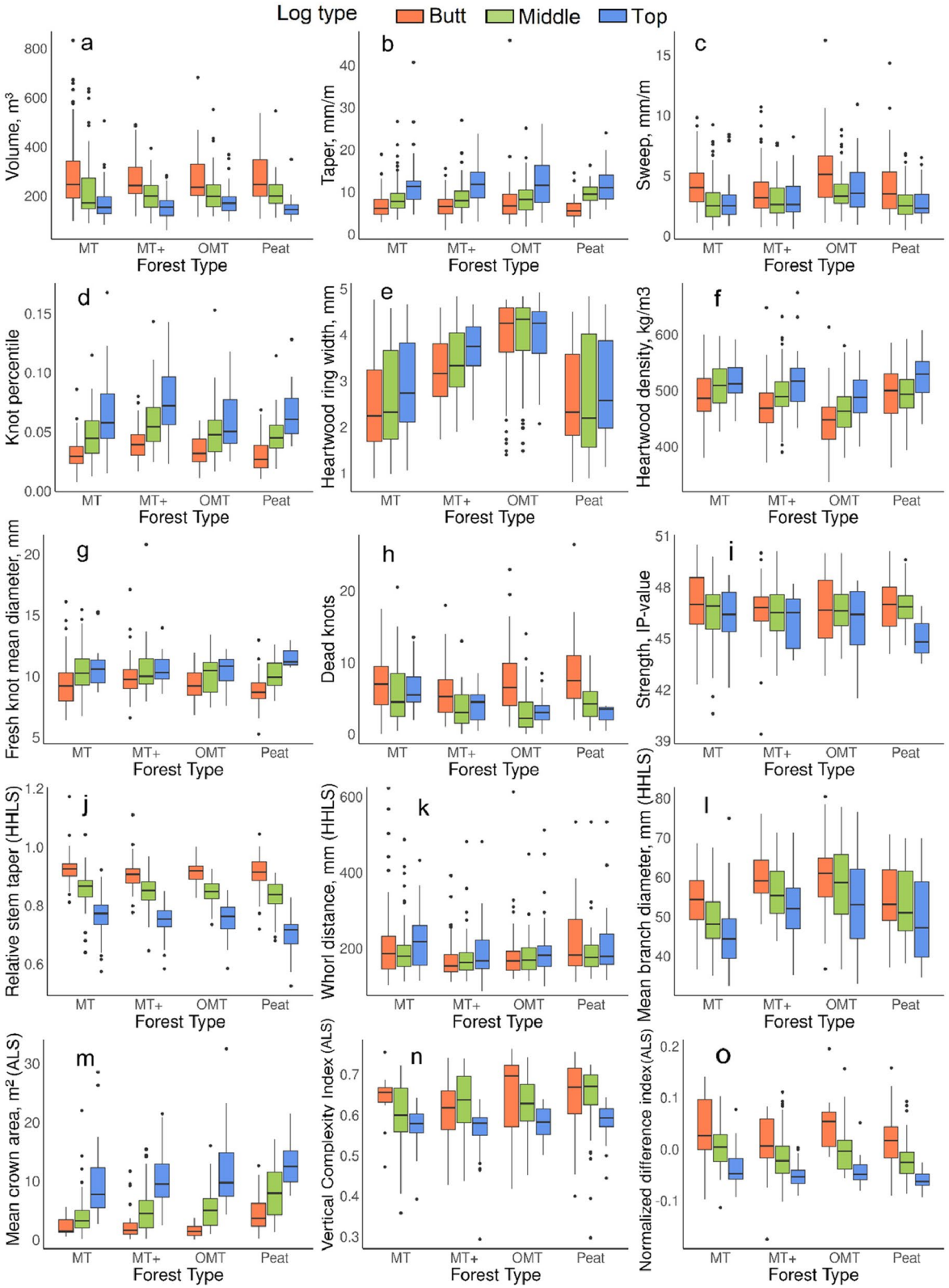

Fig. 4 The variability of selected wood quality variables from X-ray (subfigures **a**–**f**) and timber grading (subfigures **g**–**i**) measurements, along with wood quality indicators from handheld and airborne laser scanning (HHLS and ALS, subfigures **j**–**l** and **m**–**o**, respectively) per forest type (according to the Finnish system: OMT = herb-rich, Oxalis-Myrtillus type, MT/MT+ = mesic Myrtillus type) and log type (butt, middle, and top)

Table 6 The most important wood quality predictors across the hierarchical levels and data sources according to Random Forest. See Table 2 for variable abbreviations. Shaded cells highlight features that appeared most frequently among the most important predictors in Random Forests for each target variable

			X-ray											Timber grading							
			Geometry				HW			Knottiness				Knottiness							
Hierarchy	Data source	Feature	Log volume	Taper	Sweep	Crook	Heartwood volume	Heartwood density	Heartwood ring width	Knot whorls	Mean whorl distance	Knot percentage	Mean whorl volume	Dead knots	Dead knot max d	Dead knot mean d	Fresh knots	Fresh knot max d	Fresh knot mean d	Strength IP value	Total
STAND	Field	*Volume*	1	0	0	0	0	1	1	0	0	0	0	0	1	0	0	0	0	1	5
		spruceM	0	0	0	0	0	0	0	1	1	0	1	1	0	0	0	0	0	0	4
		ForestT	0	0	1	0	0	0	0	0	0	1	0	0	0	1	0	0	1	0	4
		pine-%	0	1	0	1	0	0	0	0	0	0	0	0	0	0	1	0	0	0	3
		broadl-	0	0	0	0	1	0	0	0	0	0	0	0	0	0	0	0	0	0	1
		StemsPe	0	0	0	0	0	0	0	0	0	0	0	0	0	0	0	1	0	0	1
TREE	Field	*DBH*	1	1	0	0	1	1	1	0	1	1	0	1	1	1	0	0	0	1	11
		DBHRel	0	0	0	0	0	0	0	1	0	0	1	0	0	0	1	0	1	0	4
		DBHRel	0	0	1	1	0	0	0	0	0	0	0	0	0	0	0	1	0	0	3
	ALS geometric	*CrVol*	1	1	0	0	0	0	0	0	1	1	0	0	0	0	0	0	1	0	5
		Zpcum9	0	0	0	0	0	1	0	0	0	0	0	1	0	0	1	0	0	0	3
		Zmean	0	0	0	0	0	0	1	0	0	0	1	0	0	0	0	0	0	0	2
		CrVolU	0	0	0	0	1	0	0	1	0	0	0	0	0	0	0	0	0	0	2
		CGFsd	0	0	0	0	0	0	0	0	0	0	0	0	0	0	0	0	0	1	1
		VCI	0	0	1	0	0	0	0	0	0	0	0	0	0	0	0	0	0	0	1
		Zpcum5	0	0	0	1	0	0	0	0	0	0	0	0	0	0	0	0	0	0	1
		CGFske	0	0	0	0	0	0	0	0	0	0	0	0	1	0	0	0	0	0	1
		LADsd	0	0	0	0	0	0	0	0	0	0	0	0	0	1	0	0	0	0	1
		CPAmax	0	0	0	0	0	0	0	0	0	0	0	0	0	0	0	1	0	0	1
	ALS spectral	*NIR1_1s*	0	0	0	0	0	0	0	0	0	0	0	0	0	0	1	1	0	1	3
		NIR1_is	0	0	0	0	0	1	0	0	0	0	0	0	0	1	0	0	1	0	3
		NIR1_1s	1	0	0	0	1	0	1	0	0	0	0	0	0	0	0	0	0	0	3
		NIR1_is	0	0	0	0	0	0	0	0	0	0	1	1	0	0	0	0	0	0	2
		NIR1_1s	0	1	1	0	0	0	0	0	0	0	0	0	0	0	0	0	0	0	2
		NIR1_i	0	0	0	0	0	0	0	0	1	1	0	0	0	0	0	0	0	0	2
		NIR1_2	0	0	0	1	0	0	0	0	0	0	0	0	0	0	0	0	0	0	1
		NIR2_i	0	0	0	0	0	0	0	0	0	0	0	0	1	0	0	0	0	0	1
		NIRBoth	0	0	0	0	0	0	0	1	0	0	0	0	0	0	0	0	0	0	1
LOG	Sawmill	D_{buttX}	1	1	0	0	1	1	0	0	0	0	0	1	0	1	1	1	1	1	10
		D_{topX}	0	0	0	0	0	0	0	0	1	1	1	0	0	0	0	0	0	0	3
		H_{top}	0	0	1	0	0	0	1	0	0	0	0	0	1	0	0	0	0	0	3
		Length	0	0	0	1	0	0	0	1	0	0	0	0	0	0	0	0	0	0	2
	ALS geometric	*Zmax*	0	1	0	0	1	1	0	1	1	1	1	0	0	0	0	0	0	1	8
		Zmean	1	0	1	0	0	0	1	0	0	0	0	1	1	1	0	0	0	0	6
		CPAmea	0	0	0	1	0	0	0	0	0	0	0	0	0	0	0	0	0	0	1
		CrVol	0	0	0	0	0	0	0	0	0	0	0	0	0	0	0	0	1	0	1
		LADmax	0	0	0	0	0	0	0	0	0	0	0	0	0	0	0	1	0	0	1
		VM05sd	0	0	0	0	0	0	0	0	0	0	0	0	0	0	1	0	0	0	1
LOG	ALS spectral	*NDI*	1	0	0	0	0	0	0	1	1	0	1	0	0	0	0	0	0	0	4
		NIR2_i	0	1	0	0	0	0	0	0	0	1	0	0	0	0	1	0	0	0	3
		NIR1_1s	0	0	0	0	0	0	0	0	0	0	0	0	1	1	0	0	0	0	2
		NIR2_is	0	0	0	1	0	0	0	0	0	0	0	1	0	0	0	0	0	0	2
		NDVI_1	0	0	0	0	1	0	0	0	0	0	0	0	0	0	0	0	0	0	1
		NIR1_2	0	0	1	0	0	0	0	0	0	0	0	0	0	0	0	0	0	0	1
		NIR1_2	0	0	0	0	0	0	1	0	0	0	0	0	0	0	0	0	0	0	1
		NIR1_is	0	0	0	0	0	1	0	0	0	0	0	0	0	0	0	0	0	0	1
		NIR1_1s	0	0	0	0	0	0	0	0	0	0	0	0	0	0	0	1	0	0	1
		NIR1_is	0	0	0	0	0	0	0	0	0	0	0	0	0	0	0	0	1	0	1
		NIR1_la	0	0	0	0	0	0	0	0	0	0	0	0	0	0	0	0	0	1	1
	HHLS	D_{buttt}	1	0	0	0	1	1	0	1	1	0	1	0	0	0	0	0	0	0	6
		relTaper	0	1	0	0	0	0	0	0	0	1	0	1	0	0	0	0	1	0	4
		max	0	0	0	1	0	0	1	0	0	0	0	0	0	0	0	0	0	0	2
		mean	0	0	1	0	0	0	0	0	0	0	0	0	0	0	0	1	0	0	2
		max	0	0	0	0	0	0	0	0	0	0	0	0	0	0	1	0	0	0	1
		knotVol	0	0	0	0	0	0	0	0	0	0	0	0	0	1	0	0	0	0	1
		Taper	0	0	0	0	0	0	0	0	0	0	0	0	0	0	0	0	0	1	1
		max	0	0	0	0	0	0	0	0	0	0	0	0	1	0	0	0	0	0	1

The relative taper value derived from HHLS was also an important indicator of dead knot levels (Table 6); in all groups except MT+top logs, the more cylindrical the log shape, the more dead knots in the core timber (Fig. 5b7). Moreover, an increasing mean branch diameter in HHLS indicated fewer dead knots, except in peatland top logs. The number of dead knots correlated poorly with whorl distance (Fig. 5c7).

At the tree level, the ALS-derived statistics of *CGF* and *LAD* were good predictors for dead knot presence and size (Table 6). However, the best ALS-derived indicator at the log level was related to tree height (*Zmean*) (Table 6). Indeed, increasing crown area indicated fewer dead knots in all groups except OMT top logs (Fig. 5d7). Increased vertical complexity and *NDI* generally indicated more dead knots at the log level (Fig. 5e7, f7).

Table 7 The performance of predictor variable feature spaces in predicting wood quality variables in the test data using Random Forest; mean coefficients of determination (R^2) and root-mean-squared errors relative to the reference mean (RMSE-%) from 100 Random Forests fitted to random subsamples of the data. The results indicate the transferability of the models at the stand, tree, and log levels. Cell colors indicate the explanatory power and accuracy of the respective models (R^2: red = lower explanatory power, green = higher explanatory power. RMSE-%: red = higher RMSE-%, green = lower RMSE-%)

		Hierarchy →	LOG+TREE		LOG								TREE						STAND	
Group		Feature space →	HHLS+ALS		HHLS		ALS spectr.		ALS geom.		Sawmill		ALS spectr.		ALS geom.		Field		Field	
		Variable ↓ Statistic →	R^2	RMSE-%	R^2	RMSE-%	R^2	RMSE-%	R^2	RMSE-%	R^2	RMSE-%	R^2	RMSE-%	R^2	RMSE-%	R^2	RMSE-%	R^2	RMSE-%
X-ray	Geometry	Log volume (m^3)	0.83	19.50	0.84	17.50	0.14	42.10	0.23	40.60	0.96	8.50	0.18	43.20	0.17	44.90	0.22	40.00	0.04	44.30
		Taper (cm/m)	0.23	43.10	0.21	45.70	0.10	44.60	0.18	39.00	0.22	43.70	0.02	54.90	0.02	55.40	0.01	57.40	0.01	50.10
		Sweep (cm/m)	0.09	52.80	0.07	58.70	0.01	53.80	0.03	54.10	0.04	59.40	0.08	56.30	0.08	62.30	0.08	55.90	0.05	58.40
		Crook (mm/ 2 m)	0.12	45.30	0.06	47.10	0.01	46.80	0.01	50.70	0.02	50.00	0.11	49.10	0.13	47.90	0.12	48.40	0.08	42.10
	HW	Heartwood volume (m^3)	0.76	29.40	0.76	30.70	0.17	63.20	0.19	67.80	0.85	24.10	0.18	62.70	0.18	69.30	0.20	63.80	0.10	65.50
		Heartwood density (kg/m3)	0.24	8.50	0.22	8.90	0.04	9.70	0.09	9.50	0.16	9.50	0.15	9.40	0.15	9.40	0.21	9.20	0.18	9.20
		Heartwood ring width (index)	0.51	23.70	0.34	27.50	0.14	27.30	0.05	27.60	0.04	34.50	0.62	20.10	0.62	19.70	0.60	21.20	0.55	21.70
	Knottiness	Knot whorls (n)	0.25	26.70	0.25	28.70	0.02	31.40	0.04	32.10	0.29	27.90	0.10	31.70	0.11	33.00	0.15	32.80	0.08	31.70
		Mean whorl distance (cm)	0.24	32.30	0.22	31.50	0.02	35.00	0.06	34.30	0.20	31.70	0.21	31.30	0.23	32.40	0.22	31.40	0.08	34.40
		Knot index (percentage)	0.38	39.80	0.32	40.70	0.12	43.30	0.21	40.20	0.25	44.00	0.14	47.40	0.13	47.70	0.14	45.60	0.06	48.70
		Mean whorl volume (cm3)	0.28	47.30	0.28	42.30	0.14	46.40	0.22	43.70	0.35	46.20	0.02	61.30	0.02	56.40	0.01	60.30	0.02	51.80
Timber grading	Knottiness	Dead knots (n)	0.15	60.20	0.13	65.60	0.02	66.30	0.03	75.20	0.09	69.70	0.08	72.60	0.09	68.50	0.05	66.10	0.14	58.60
		Dead knot max d (cm)	0.01	134.90	0.01	113.00	0.02	113.40	0.01	213.30	0.01	117.10	0.01	122.80	0.01	134.00	0.01	129.10	0.02	114.30
		Dead knot mean d (cm)	0.01	70.40	0.01	69.60	0.02	66.90	0.02	72.00	0.01	70.10	0.01	78.30	0.01	77.40	0.01	77.30	0.03	64.50
		Fresh knots (n)	0.17	27.30	0.15	27.80	0.02	25.70	0.04	27.30	0.14	26.50	0.13	26.20	0.10	28.50	0.09	27.60	0.12	28.00
		Fresh knot max d (cm)	0.02	37.50	0.02	43.80	0.02	39.70	0.02	36.10	0.01	46.30	0.02	41.30	0.03	38.50	0.02	46.00	0.01	48.80
		Fresh knot mean d (cm)	0.19	16.10	0.12	17.20	0.02	16.20	0.02	16.00	0.12	16.80	0.10	17.20	0.11	16.50	0.08	18.00	0.03	18.40
		Strength (IP value)	0.05	3.80	0.06	3.80	0.02	3.60	0.02	3.70	0.03	3.90	0.03	4.00	0.03	4.00	0.03	4.10	0.01	3.90
Mean			0.25	39.9	0.23	40.0	0.06	43.1	0.08	49.1	0.21	40.6	0.12	46.1	0.12	47.0	0.13	46.3	0.09	44.1
Standard deviation			0.24	29.37	0.23	25.68	0.06	25.16	0.08	45.48	0.27	27.39	0.14	28.50	0.14	30.31	0.14	29.02	0.12	25.28

HHLS handheld laser scanning, *ALS* airborne laser scanning, *geom. and spectr* geometrical and spectral (905 nm and 1550 nm) features, respectively, *RMSE* root-mean-squared error, *HW* heartwood, *d* diameter

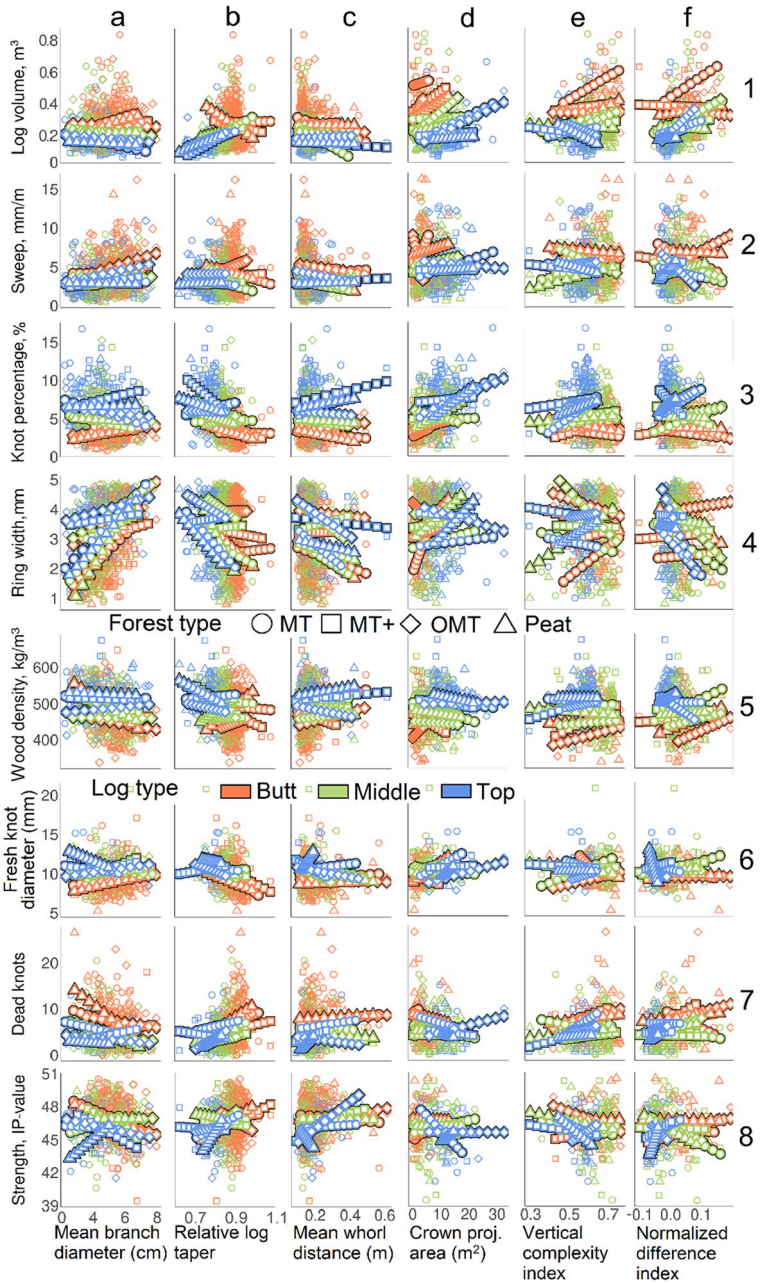

Fig. 5 Relationships between selected log-level features measured from handheld (HHLS) and aerial (ALS) laser-scanned point clouds (on the *x*-axis: mean branch diameter, relative log taper, and mean whorl distance from HHLS, and crown projection area, vertical complexity index and normalized difference index from ALS) and wood and timber quality features measured at the sawmill (on the *y*-axis: log volume, sweep, knot percentage, and heartwood mean ring width and wood density with X-rays, and mean fresh knot diameter, number of dead knots, and timber strength IP value from the photogrammetric grading of the core timber). The relationships are presented separately for each log type (butt, middle, and top) and forest type (according to the Finnish system: OMT = herb-rich, Oxalis-Myrtillus type, MT/MT+ = mesic Myrtillus type)

3.2.4 Heartwood properties

More conical stem shape and larger crown areas typically resulted in wider rings and higher wood density (Fig. 5b4, b5, d4, d5). Mean branch diameters were strongly and positively correlated with ring widths (Fig. 5a4) but had a less clear relationship with wood density (Fig. 5a5). Timber strength IP value in general decreased with increasing branch diameters, although the peatland top logs showed an exemption to this rule (Fig. 5a8). A moderate positive correlation was

observed between timber strength IP and whorl-to-whorl distance, particularly in the top logs (but excluding peatlands) (Fig. 5c8). A larger relative log taper (more cylindrical logs) was associated with larger timber strength IP in the top logs and MT+ and peatland butt logs but showed a negative correlation with timber strength IP in other logs (Fig. 5b8).

NDI correlated slightly positively with wood density in butt logs and middle logs (Fig. 5f5) and negatively with ring width in the top logs and middle logs (Fig. 5f4). Crown properties also reflected variations in timber strength (Fig. 5d8, e8) across log positions and forest types. Trends between strength IP value and *VCI* were less obvious (Fig. 5f8).

3.3 Robustness and transferability of log-level wood and timber property predictions

The transferability of the RF models to the test data was remarkably lower than that indicated by the total variance level explained by the various hierarchical levels in the LMEMs or the explanatory powers of the different feature spaces in the RF training data (Table 8, in Appendix).

The wood quality predictions made with the HHLS features outperformed the other data sources in the extrapolation to the test data, with an average R^2 of 0.32 and an RMSE of 35% for the X-ray variables and an R^2 of 0.04 and an RMSE of 43% for the sawn timber variables (Table 7). Best performance was obtained for the log volume and heartwood volume predictions with the HHLS features (R^2 0.78 and 0.72 and RMSE 21% and 34%, respectively) (Table 7).

The log-level ALS features were less robust predictors than the HHLS features: R^2 was 0.13 with geometrical ALS features and 0.07 with spectral ALS features for the X-ray variables and 0.02 with both in the sawn timber variables (Table 7).

All feature spaces yielded similar RMSEs for the core timber fresh knot mean diameter and timber strength IP (approximately 12–18%) and for timber strength IP value (4%) (Table 7). It is noteworthy that timber strength IP exhibited a rather low level of variability in the data, with a standard deviation of 3% of the mean.

After testing various combined feature spaces at both the log and tree levels, we found that the combination of log-level HHLS features and tree-level ALS features (both geometrical and spectral) slightly improved the robustness and transferability of the prediction from those achieved with the sole HHLS features (Table 7). For example, heartwood ring width (R^2: 0.51, RMSE 24%), heartwood density (R^2: 0.24, RMSE: 8.5%), and knot percentage (R^2: 0.38, RMSE: 40%) gave relatively good responses to the combined use of ALS and HHLS features.

The issues related to the robustness and transferability of the wood quality models based on size- and growth-related tree features are also interpretable from the appearance of the trees studied here (Fig. 3). We observed that some trees, despite sharing macro-level resemblance, may differ in wood density, e.g., the two example trees in MT+ were similar in size, mean branch diameter, *NDI* and *VCI*, and ring width, but different in mean heartwood densities (416 kg m^{-3} vs. 571 kg m^{-3}) (Fig. 3, MT+). On the other hand, some trees with rather similar wood properties differed in their exterior appearance, e.g., two trees from MT and MT+ that had similar heartwood density (571 kg m^{-3}) but different mean branch diameters, *NDI,* and ring width (Fig. 3, right-side MT, right-side MT+).

4 Discussion

4.1 How is the variation in wood properties and laser-scanned wood quality indicators in Norway spruce hierarchically distributed across spatial levels?

With respect to our first research question, we found that most of the wood quality variability was due to within-tree factors that accounted for 73% of the variance in the data according to LMEM.

Relating to our second research question, the ALS- and HHLS-derived wood quality indicators aligned with these directions of variance, with roughly 70–90% of the variability occurring within trees.

Across all forest types, the synchronous morphosis of crown geometry and stem shape was one of the most distinguishable trends observed in the point clouds. The increased conicity of the butt logs (more bottom-heavy stems) was associated with long and large live crowns, indicating continued rapid growth in the lower stems. This was also reflected in the greater branch diameters in the conical butt logs. Together, the relative stem taper and branch diameters from HHLS were good indicators for growth rate-associated variables, e.g., ring width, higher knot percentage, and larger knots in almost all groups (Table 6).

Forest type and stand-level factors generally held minor importance to wood quality, although their effect on the growth rate was evident (Table 5).

The most fertile stands (OMT and to some extent MT+) showed signs of higher growth rates in terms of ring widths and larger branch sizes and knot percentages, along with slightly lower heartwood densities. However, the higher growth rates in the OMT stands were not pronouncedly reflected in the knot sizes (Fig. 4g) or strength IP of the timber (Fig. 4i). The high growing stock densities in the OMT stands (Table 1) likely had

effectively alleviated some of the effects associated with higher growth rates. The denser spacing was evident in the higher frequency of the dead knots in the core timber of the butt logs (Fig. 4h), indicating early branch mortality due to shading. The OMT butt logs had the largest branch diameters, indicating that the dead branches also remained attached to the stems throughout the years, which could explain the more severe sweeping of these logs (Figs. 4c and 5a2) via the distorting effect on the stem grain.

The top logs from peatlands differed from the rest of the material in that they had the least strong IP values (Fig. 4i) and largest fresh knots in the core timber (Fig. 4g). It is also worth noting that the HHLS data did not indicate a larger branch size for these logs (Fig. 4l) but instead suggested a negative correlation between the HHLS branch diameters and core timber knot size (Fig. 5a6). The HHLS also showed that these logs had the most conical shape (Fig. 4j). Peatland trees also had the widest crowns according to the ALS data (Fig. 4m). These observations could indicate the effects of the excessive soil water and the need for higher respiration, hence the large knots, wide crowns, and more conical stems. Nevertheless, the peatland trees had similar ring widths and wood densities as the MT trees did (Fig. 4e, f), underscoring the difficulty of linking external characteristics of Norway spruces with their interior wood quality.

Our observations generally aligned well with the current wood scientific consensus regarding the directions of variability in wood quality (Eberhardt et al. 2019; Jyske et al. 2014; Moore et al. 2009). The baseline effects due to stem and crown sizes affect the hydraulic and mass-bearing requirements of the trees, with implications for all wood property variables. Moreover, the growth, decline, death, and branch pruning that morph the positions and dimensions of the live and dead crowns contribute drastically to within-tree wood quality variation (Moberg 2006; Mäkinen et al. 2003).

Groot and Luther (2015) analyzed black spruce and balsam fir trees and their wood density variability at the plot, tree, and ring levels. While they found that over 50% of wood density variability occurred at the ring level (within trees), they also highlighted the aggregated effects of elevated growth rates on wood density at all levels of hierarchy. Although we also found evidence that tree size and growth rate descriptors were important (e.g., in the most fertile OMT stands), the level of variance explained at these higher hierarchical levels for ring width, total log-level wood density, and most of the wood quality variables was much smaller than those found for knot-free stemwood density by Groot and Luther (2015).

4.2 To what extent can wood quality models based on above- and below-canopy laser scanning predict the wood properties of Norway spruce?

Regarding the third research question, the laser-scanned features explained a major portion of the wood quality variability in the training data (Table 8, in the Appendix). The most important wood quality predictors were related to tree size, growth rate (as indicated, e.g., by branch diameters and stem conicity), and within-tree position. These factors resulted in similar explanatory powers in the training data regardless of the data source.

Côté et al. (2021) showed that tree-level structural information from laser scanning improved wood property models in black spruce and balsam fir trees compared with the use of traditional forest inventory attributes. They also found that the most important predictors were related to crown geometry, branching structure, stem form, and competition. However, they underlined the difficulty of establishing robust relationships between tree characteristics using linear parametric approaches, which in part inspired our use of RF to avoid problems caused by several collinear and potentially non-normally distributed predictor variables. Côté et al. (2021) found that the best models in their data were nonparametric partial least square models. With the best models, they were able to explain 12–56% of the tree-level mean wood fiber attributes. Although the wood property variables they observed differed from ours, were generalized to the tree level, and were obtained from ring samples (as opposed to the X-rayed sawlogs in our study), some common ground can be found. Our best models predicted the ring width with $R^2 = 0.51$, which is closely related to the radial tracheid diameter and cell wall thickness; variables that Côté et al. predicted with a similar accuracy at the tree level ($R^2 = 0.52$ and 0.47, respectively). Noteworthily, Giroud et al. (2019) had observed similar explanatory powers with TLS models and environmental variables for similar wood fiber attributes, indicating that the tree-level structural data indeed has the capacity of depicting relevant environmentally controlled drivers of wood property variation.

Therefore, we would expect that our approach could achieve similar accuracy also for the log-level mean wood density of the stemwood (R^2 being 0.56 in Côté et al. (2021)), it being majorly influenced by radial tracheid diameters and cell wall thickness. Wood density in our study differed from the wood density measured from knot-free ring samples in that the whole-log density also

incorporates knots that are denser than stemwood. It is worth noting that within forest types, the wood density increased towards the top logs (Fig. 4f) regardless of the wider rings (Fig. 4e), indicating that the X-ray heartwood density reflected the knot percentage (Fig. 4d) to an important degree (knot wood being denser than stemwood). As a result, the prediction accuracy of the wood density in our study ($R^2 = 0.24$) was similar to that of the knottiness variables (R^2: 0.24–0.32).

4.3 How robust are the wood quality models based on above- and below-canopy laser scanning across different forest stands?

In answer to our fourth and perhaps most pressing research question, significant overfitting evidently occurred during the RF model training, since the prediction accuracies decreased clearly in the test data (Table 7), especially with the ALS features. A large proportion of the log-to-log wood quality variances in the Norway spruces appeared stochastic enough by nature to remain elusive to descriptors captured in the point clouds. In other words, the relationships of wood properties with tree size and crown dimensions in Norway spruces are rather fluid, and the external characteristics of the Norway spruce cannot robustly depict the internal wood qualities (see, e.g., Figs. 3 and 5).

In light-demanding and plastic species, such as Scots pine, the external characteristics are often strongly correlated with wood properties (Kankare et al. 2022; Pyörälä et al. 2019a). However, in species with low crown plasticity, such as Norway spruce, the situation appears somewhat more complex.

Nevertheless, we obtained promising accuracies; for example, when extrapolating the log and heartwood volumes, knot indexes, and heartwood ring widths of the Norway spruce trees into external test data using the combination of log-level HHLS features and tree-level ALS features.

Previous studies have stressed that tree-level detailed structural data resolved from ALS and TLS point clouds improve the accuracy of wood property models (e.g., Côté et al. 2021; Groot and Luther 2015). However, based on our results, we argue that a significant portion of the true wood quality variability remains elusive to models based solely on the morphological traits of trees—especially in species with low crown plasticity such as Norway spruce, black spruce, and balsam fir. Our careful visual analysis of the data revealed important constraints regarding the complex wood quality variations across the scale, i.e., from log types to forest types (Figs. 4 and 5).

4.4 Outlook for the future

A previous study on HHLS (Winberg et al. 2023) showed that the HHLS method is comparable with TLS when considered as a tool to produce stem and branching features to serve as wood quality indicators (as opposed to reproducing complete reconstructions of the branching), despite its greater stochastic noise, lower point density, and larger footprint. The main reason we used HHLS in this study was because these point clouds resemble those achievable from laser scanners mounted on intra- or under-canopy flying drones (i.e., UAV-LS) (Hyyppä et al. 2020a; Puliti et al. 2023) and harvesters (Sagar et al. 2024).

Moreover, our high-density ALS data collected from a helicopter bears closer resemblance to drone-borne above-canopy data. Thanks to recent advances in these frontiers, similar data as that used in our study could thus soon be collected autonomously at variable heights from several trajectories through the stands to improve the point cloud coverage, density, and footprint—especially in the vertical direction. For instance, (Hyyppä et al. 2022) extracted the stem curves and Cattaneo et al. (2024) and Puliti et al. (2023) also extracted the branch whorls from UAV-LS point clouds.

Previously, comparative studies by Qi et al. (2022) and Hyyppä et al. (2020c) evaluated UAV-LS and below-canopy MLS in extracting stem and branch structures. Qi et al. (2022) found that fusing the two point cloud sources offered the most accurate depiction of complete tree structures. Hyyppä et al. (2020c) concluded that under-canopy systems provide the most accurate and comprehensive stem curve data, whereas above-canopy systems are better suited for deriving accurate tree height. These developments hold promise for the constitution of large-scale datasets that combine laser scans, harvester data, and sawmill data for upfront wood quality estimation and wood procurement planning in the industrial setting.

Mapping wood properties in standing timber using fused remote sensing and industrial data can potentially improve the flexibility and precision of forest management and use—thus contributing to a more precise and flexible choice of raw materials, wood usage optimization, and to accelerating the sustainability transition of the forest industries via improved resource-use efficiency and forest management flexibility. There are many ways to utilize the improved information on wood properties. Increasingly, harvested wood is distributed between various processors, each with their own requirements for the wood. In other words, "wood quality" in terms of superiority or inferiority—and thus the production value—can differ for the same batch of wood depending on the end user. To ensure proper incentive for optimally targeting

the harvesting operations, bucking the stem, and distributing the log products, the wood property estimation in standing timber must be compatible with tools that enable optimizing log breakdown according to various end user requirements. The performance of the sawn timber in long-term structural applications is crucial for the sustainability of the forest industries. Therefore, the maximal deposition of wood harvested to sawmilling is one of the most sought-after outcomes of enhanced forest use and was selected herein as the starting point for researching laser scanning applications in wood property estimations.

5 Conclusion

Our hypothesis was that partitioning the feature space—both for the response and predictor variables—at the within-tree level would increase the explanatory powers of the models. However, this hypothesis proved wrong for most wood quality variables in Norway spruce. In our study, approximately 73% of the wood quality variation occurred within trees, but the relationships with external tree features were dependent on stand conditions and forest type. We found it challenging to establish robust and transferable wood quality models with Norway spruce, which shows relatively little plasticity in its crown development. However, the positive exceptions were log-level heartwood volume, ring width, and knot percentage for which within-tree modeling did lead to promising explanatory performance when transferred from training data to test data. By contrast, tree species with higher light demand and/or more plastic crowns are likely better suited for laser scanning-based wood property estimations at the tree level.

Based on our findings, the fusion of complementary data sources to improve our understanding of wood quality should concentrate on capturing the within-tree variability of wood properties across variable species and growth conditions. This could be achieved by utilizing laser scanning systems that are increasingly autonomous and can operate both above and below forest canopies, accompanied by sufficient references of wood quality to enable the establishment of empirical models or calibration of process-based models that are often used to derive large-scale maps of forest growth and carbon uptake.

Appendix

Table 8 The performance predictor variable feature spaces in explaining the variance of the target wood quality variables with Random Forest in the training data; mean coefficients of determination (R^2) and root-mean-squared errors relative to the reference mean (RMSE-%) from 100 Random Forests fitted to random subsamples of the data. HHLS: handheld laser scanning, ALS: airborne laser scanning, geom. and spectr.: geometrical and spectral (905 nm and 1550 nm) features, respectively, HW: heartwood, d: diameter. Cell colors indicate the explanatory power and accuracy of the respective models (R2: red = lower explanatory power, green = higher explanatory power. RMSE-%: red = higher RMSE-%, green = lower RMSE-%)

		Hierarchy →	LOG+TREE		LOG								TREE						STAND	
Group		Feature space →	HHLS+ALS		HHLS		ALS spectr.		ALS geom.		Sawmill		ALS spectr.		ALS geom.		Field		Field	
		Variable ↓ Statistic →	R^2	RMSE-%	R^2	RMSE-%	R^2	RMSE-%	R^2	RMSE-%	R^2	RMSE-%	R^2	RMSE-%	R^2	RMSE-%	R^2	RMSE-%	R^2	RMSE-%
X-ray	Geometry	Log volume (m^3)	0.98	7.20	0.98	7.10	0.94	15.90	0.94	15.00	1.00	3.20	0.59	29.80	0.59	29.50	0.59	29.00	0.07	42.90
		Taper (cm/m)	0.94	16.60	0.94	17.60	0.95	16.70	0.94	16.30	0.92	18.10	0.46	36.70	0.46	36.60	0.40	39.40	0.03	50.20
		Sweep (cm/m)	0.94	22.40	0.96	20.90	0.97	20.50	0.96	20.30	0.93	22.20	0.62	36.10	0.62	35.10	0.62	35.80	0.07	54.00
		Crook (mm/ 2m)	0.93	19.00	0.95	18.40	0.97	19.70	0.97	19.20	0.95	19.10	0.65	31.00	0.64	31.40	0.65	28.90	0.09	46.90
	HW	Heartwood volume (m^3)	0.97	12.50	0.97	12.30	0.94	25.30	0.94	24.40	0.98	9.60	0.59	44.00	0.59	42.80	0.60	40.60	0.11	59.80
		Heartwood density (kg/m^3)	0.94	3.20	0.94	3.40	0.96	3.60	0.94	3.60	0.92	3.70	0.64	6.00	0.64	6.00	0.68	5.80	0.21	9.00
		Heartwood ring width (index)	0.93	10.20	0.95	10.10	0.95	10.10	0.96	10.80	0.94	12.90	0.87	11.70	0.87	11.70	0.87	12.20	0.55	22.30
	Knottiness	Knot whorls (n)	0.95	10.50	0.94	10.70	0.97	12.10	0.95	11.90	0.93	10.70	0.59	20.50	0.59	20.30	0.62	20.50	0.11	31.10
		Mean whorl distance (cm)	0.95	11.60	0.94	11.90	0.97	12.80	0.96	12.50	0.93	12.40	0.69	19.90	0.69	19.80	0.69	20.10	0.11	33.40
		Knot index (percentage)	0.95	15.00	0.95	15.90	0.95	16.50	0.93	15.80	0.92	16.90	0.59	32.90	0.59	32.80	0.59	33.30	0.08	48.50
		Mean whorl volume (cm^3)	0.94	16.90	0.94	17.30	0.95	17.30	0.93	16.70	0.93	16.30	0.49	37.60	0.50	38.30	0.48	37.80	0.05	51.30
Timber grading	Knottiness	Dead knots (n)	0.94	24.30	0.95	25.00	0.96	27.70	0.94	27.00	0.93	26.20	0.73	37.00	0.73	37.50	0.72	39.80	0.18	64.70
		Dead knot max d (cm)	0.95	50.60	0.96	50.00	0.95	56.90	0.95	50.00	0.94	52.10	0.61	82.70	0.61	80.10	0.60	81.50	0.05	121.00
		Dead knot mean d (cm)	0.95	26.30	0.96	25.90	0.96	24.50	0.96	24.70	0.94	27.00	0.61	40.60	0.62	40.50	0.58	42.60	0.06	62.50
		Fresh knots (n)	0.94	9.80	0.95	9.90	0.97	10.50	0.96	10.00	0.94	10.50	0.77	14.60	0.76	14.50	0.76	15.20	0.16	26.00
		Fresh knot max d (cm)	0.93	16.40	0.97	19.30	0.97	16.30	0.90	19.20	0.95	19.90	0.80	19.50	0.80	19.60	0.74	26.70	0.04	45.90
		Fresh knot mean d (cm)	0.93	6.40	0.95	6.50	0.98	6.30	0.96	6.30	0.93	6.60	0.74	9.20	0.74	9.30	0.70	10.30	0.07	17.20
		Strength (IP value)	0.93	1.40	0.96	1.40	0.97	1.30	0.96	1.40	0.94	1.50	0.67	2.20	0.66	2.20	0.65	2.30	0.05	3.70
Mean			0.94	15.6	0.95	15.8	0.96	17.4	0.95	17.0	0.94	16.1	0.65	28.4	0.65	28.2	0.641	29.0	0.12	43.9
Standard deviation			0.01	11.12	0.01	10.98	0.01	12.18	0.02	10.85	0.02	11.71	0.10	18.62	0.10	18.13	0.10	18.27	0.12	26.36

Acknowledgements
The study materials used in this study were provided by courtesy of Stora Enso Metsä oyj (SE) and Finnos oy. We acknowledge Pekka Alajärvi, Mika Korvenranta (currently with CollectiveCrunch oy), and Kalle Kärhä (currently with the University of Eastern Finland) from SE for their contribution to project planning, data acquisition, and joint seminar organization. Moreover, several additional people from SE and their contractors deserve our sincere thanks for making this study happen and for granting us their expertise, including but not limited to Timo Rauhansalo, Titta Laitinen, Pasi Vanhatalo, Juha Jousinen, Harri Manula, Tiina Ruuskanen, Markus Ylönen, Markku Salminen, Jarmo Kilpiä, and Janne Kuusisto. Juha Alatalo from Finnos is acknowledged for information regarding the principles and performance of the X-ray scanning. Dr. Cristoffer Axelsson from the Swedish University of Agricultural Sciences is acknowledged for help and ideas with ALS feature extraction. Dr. Samuli Junttila from the University of Eastern Finland (currently with University of Helsinki) assisted with the registration of the TLS scans. The high-performance computing environments provided by the CSC - IT Center for Science Ltd. were utilized in the data processing and statistical analyses. The language was edited by Stella Thompson.

Authors' contributions
JP wrote the first version of the manuscript, designed the study plan and research questions, carried out and managed key parts of the fieldwork and data processes, and conducted the statistical analysis. MP participated in the fieldwork, contributed to the preprocessing of the sawmill data and the preliminary statistical analyses. OS designed and carried out the stem taper modeling procedure and the stem variable extraction. OW carried out the treeQSM data processing phase for raw stem measurements and branch observations. XY supervised the stem and branching extractions from HHLS and participated in the ALS data processing and data fusion between ALS and HHLS. HK and AK planned and carried out the collection of the HHLS and ALS data and preprocessed these data. JP, MH, HK, AK, Jho, and JHy were responsible for the original research plans, funding acquisition, and project management. All authors have read and edited the manuscript and agreed upon its contents.

Funding
Open Access funding provided by University of Helsinki (including Helsinki University Central Hospital). This study was funded jointly by the following research grants: Research Council of Finland (formerly the Academy of Finland) Proof-of-Concept project "Advanced Laser Scanning for Enhanced Wood Quality Mapping and Value Chain Optimization" (Forest2Factory) [365360], Tandem Forest Values – project "Estimating Forest Resources and Quality-related Attributes Using Automated Methods and Technologies" (ForestQuality) [334829, 334830], "Feasibility of Inside-Canopy UAV Laser Scanning for Automated Tree Quality Surveying" (Quality4Trees) [334002], "Understanding Wood Density Variation Within and Between Trees using Multispectral Point Cloud Technologies and X-ray microdensitometry" (Density4Trees) [331708], "Forest-Human-Machine Interplay - Building Resilience, Redefining Value Networks and Enabling Meaningful Experiences" (UNITE) [337656] flagship, as well as the Ministry of Agriculture and Forestry grant: "Future forest information system at individual tree level" [VN/3482/2021].

Data availability
The point clouds used in this study are openly reposited in the Fairdata Etsin service:
- Pyörälä, J., Hyyppä, J., Kukko, A., & Kaartinen, H. (2026). Dense Airborne Laser Scanning point clouds from southeastern Finland (Version 1). University of Helsinki. https://doi.org/10.23729/fd-b7151c1a-6959-3fb3-af27-586f9ca415e6
- Pyörälä, J., Hyyppä, J., Kukko, A., & Kaartinen, H. (2026). Dense Handheld Laser Scanning point clouds from southeastern Finland (Version 1). University of Helsinki. https://doi.org/10.23729/fd-0a21c7cc-1df5-302d-927e-eacf72857f07
The rest of the research materials of this study are available from the corresponding author (JP), but restrictions apply to the availability of the industrial data, which were used under license for the current study and so are not publicly available due to proprietary reasons. The data are, however, available upon request and with permission from the Finnish Geospatial Research Institute (FGI).

Declarations

Ethics approval and consent to participate
Not applicable.

Competing interests
The authors declare no competing interests.

Author details
[1]Department of Photogrammetry and Remote Sensing, Finnish Geospatial Research Institute, Espoo, Finland. [2]Department of Forest Sciences, University of Helsinki, Helsinki, Finland. [3]Department of Forest Sciences, University of Eastern Finland, Joensuu, Finland. [4]Department of Forest Ecology and Management, Swedish University of Agricultural Sciences, Umeå, Sweden.

Received: 10 September 2025 Accepted: 26 February 2026
Published online: 14 March 2026

References

Achim A, Moreau G, Coops NC, Axelson JN, Barrette J, Bédard S, Byrne KE, Caspersen J, Dick AR, D'Orangeville L (2022) The changing culture of silviculture. Forestry 95(2):143–152. https://doi.org/10.1093/forestry/cpab047
Babst F, Bodesheim P, Charney N, Friend AD, Girardin MP, Klesse S, Moore DJP, Seftigen K, Bjorklund J, Bouriaud O, Dawson A, DeRose RJ, Dietze MC, Eckes AH, Enquist B, Frank DC, Mahecha MD, Poulter B, Record S, Trouet V, Turton RH, Zhang Z, Evans MEK (2018) When tree rings go global: challenges and opportunities for retro- and prospective insight. Quat Sci Rev 197:1–20. https://doi.org/10.1016/j.quascirev.2018.07.009
Barrette J, Achim A, Auty D (2023) Impact of intensive forest management practices on wood quality from conifers: literature review and reflection on future challenges. Curr Forestry Rep 9:101–130. https://doi.org/10.1007/s40725-023-00181-6
Blanchette D, Fournier RA, Luther JE, Côté J-F (2015) Predicting wood fiber attributes using local-scale metrics from terrestrial LiDAR data: a case study of Newfoundland conifer species. For Ecol Manage 347:116–129. https://doi.org/10.1016/j.foreco.2015.03.013
Bouvier M, Durrieu S, Fournier RA, Renaud J-P (2015) Generalizing predictive models of forest inventory attributes using an area-based approach with airborne LiDAR data. Remote Sens Environ 156:322–334. https://doi.org/10.1016/j.rse.2014.10.004
Breiman L (2001) Random forests. Mach Learn 45(1):5–32. https://doi.org/10.1023/A:1010933404324
Büntgen U, Krusic PJ, Piermattei A, Coomes DA, Esper J, Myglan VS, Kirdyanov AV, Camarero JJ, Crivellaro A, Körner C (2019) Limited capacity of tree growth to mitigate the global greenhouse effect under predicted warming. Nat Commun 10(1):2171. https://doi.org/10.1038/s41467-019-10174-4
Cattaneo N, Puliti S, Fischer C, Astrup R (2024) Estimating wood quality attributes from dense airborne LiDAR point clouds. For Ecosyst 11:100184. https://doi.org/10.1016/j.fecs.2024.100184
Chen S, Shahi C, Chen HY (2016) Economic and ecological trade-off analysis of forest ecosystems: options for boreal forests. Environ Rev 24(3):348–361. https://doi.org/10.1139/er-2015-0090
Côté JF, Luther JE, Lenz P, Fournier RA, van Lier OR (2021) Assessing the impact of fine-scale structure on predicting wood fibre attributes of boreal conifer trees and forest plots. For Ecol Manage 479:118624. https://doi.org/10.1016/j.foreco.2020.118624
Dalponte M, Coomes DA (2016) Tree-centric mapping of forest carbon density from airborne laser scanning and hyperspectral data. Methods Ecol Evol 7(10):1236–1245. https://doi.org/10.1111/2041-210X.12575
Drew DM, Downes GM, Seifert T, Eckes-Shepard A, Achim A (2022) A review of progress and applications in wood quality modelling. Curr Forestry Rep 8(4):317–332. https://doi.org/10.1007/s40725-022-00171-0
Eberhardt TL, So C-L, Leduc DJ (2019) Wood property maps showing wood variability in mature longleaf pine: does getting old change juvenile tendencies? Wood Fiber Sci 51(2):193–208. https://doi.org/10.22382/wfs-2019-020

Edelsbrunner H, Mücke EP (1994) Three-dimensional alpha shapes. ACM Transactions on Graphics (TOG) 13(1):43–72. https://doi.org/10.1145/174462.156635

Ester M, Kriegel HP, Sander J, Xu X (1996) A density-based algorithm for discovering clusters in large spatial databases with noise. In: HJ Simoudis E, Fayyad U, editors. Second International Conference on Knowledge Discovery and Data Mining Proceedings. 96(34):226-231. https://cdn.aaai.org/KDD/1996/KDD96-037.pdf

Fischler MA, Bolles RC (1981) Random sample consensus: a paradigm for model fitting with applications to image analysis and automated cartography. Commun ACM 24(6):381–395. https://doi.org/10.1145/358669.358692

Friend AD, Eckes-Shephard AH, Fonti P, Rademacher TT, Rathgeber CB, Richardson AD, Turton RH (2019) On the need to consider wood formation processes in global vegetation models and a suggested approach. Ann Forest Sci 76(2):49. https://doi.org/10.1007/s13595-019-0819-x

Gauthier S, Bernier P, Kuuluvainen T, Shvidenko A, Schepaschenko D (2015) Boreal forest health and global change. Science 349(6250):819–822. https://doi.org/10.1126/science.aaa9092

Giroud G, Schneider R, Fournier RA, Luther JE, Martin-Ducup O (2019) Modeling black spruce wood fiber attributes with terrestrial laser scanning. Can J Forest Res 49(6):661–669. https://doi.org/10.1139/cjfr-2018-0342

Groot A, Luther JE (2015) Hierarchical analysis of black spruce and balsam fir wood density in Newfoundland. Can J Forest Res 45(7):805–816. https://doi.org/10.1139/cjfr-2015-0064

Hanhijärvi A, Ranta-Maunus A, Turk G (2005) Potential of strength grading of timber with combined measurement techniques (1235–0621). (VTT PUBLICATIONS, Volume 568). https://publications.vtt.fi/pdf/publications/2005/P568.pdf

Hartley RJ, Jayathunga S, Massam PD, De Silva D, Estarija HJ, Davidson SJ, Wuraola A, Pearse GD (2022) Assessing the potential of backpack-mounted mobile laser scanning systems for tree phenotyping. Remote Sens 14(14):3344. https://doi.org/10.3390/rs14143344

Hilker T, Frazer GW, Coops NC, Wulder MA, Newnham GJ, Stewart JD, van Leeuwen M, Culvenor DS (2013) Prediction of wood fiber attributes from LiDAR-derived forest canopy indicators. Forest Sci 59(2):231–242. https://doi.org/10.5849/forsci.11-074

Hölttä T, Mäkinen H, Nöjd P, Mäkelä A, Nikinmaa E (2010) A physiological model of softwood cambial growth. Tree Physiol 30(10):1235–1252. https://doi.org/10.1093/treephys/tpq068

Hyyppä E, Hyyppä J, Hakala T, Kukko A, Wulder MA, White JC, Pyörälä J, Yu X, Wang Y, Virtanen J-P, Pohjavirta O, Liang X, Holopainen M, Kaartinen H (2020a) Under-canopy UAV laser scanning for accurate forest field measurements. ISPRS J Photogramm Remote Sens 164:41–60. https://doi.org/10.1016/j.isprsjprs.2020.03.021

Hyyppä E, Kukko A, Kaijaluoto R, White JC, Wulder MA, Pyörälä J, Liang X, Yu X, Wang Y, Kaartinen H (2020b) Accurate derivation of stem curve and volume using backpack mobile laser scanning. ISPRS J Photogramm Remote Sens 161:246–262. https://doi.org/10.1016/j.isprsjprs.2020.01.018

Hyyppä E, Yu X, Kaartinen H, Hakala T, Kukko A, Vastaranta M, Hyyppä J (2020c) Comparison of backpack, handheld, under-canopy UAV, and above-canopy UAV laser scanning for field reference data collection in boreal forests. Remote Sens 12(20):3327. https://doi.org/10.3390/rs12203327

Hyyppä E, Kukko A, Kaartinen H, Yu X, Muhojoki J, Hakala T, Hyyppä J (2022) Direct and automatic measurements of stem curve and volume using a high-resolution airborne laser scanning system. Science of Remote Sensing 5:100050. https://doi.org/10.1016/j.srs.2022.100050

Jenness JS (2004) Calculating landscape surface area from digital elevation models. Wildl Soc Bull 32(3):829–839. https://doi.org/10.2193/0091-7648(2004)032[0829:CLSAFD]2.0.CO;2

Johansson E, Johansson D, Skog J, Fredriksson M (2013) Automated knot detection for high speed computed tomography on *Pinus sylvestris* L. and *Picea abies* (L.) Karst. using ellipse fitting in concentric surfaces. Comput Electron Agric 96:238–245. https://doi.org/10.1016/j.compag.2013.06.003

Jyske T, Mäkinen H, Saranpää P (2008) Wood density within Norway spruce stems. Silva Fenn 42(3):248. https://doi.org/10.14214/sf.248

Jyske T, Mäkinen H, Kalliokoski T, Nöjd P (2014) Intra-annual tracheid production of Norway spruce and Scots pine across a latitudinal gradient in Finland. Agric for Meteorol 194:241–254. https://doi.org/10.1016/j.agrformet.2014.04.015

Kankare V, Saarinen N, Pyörälä J, Yrttimaa T, Hynynen J, Huuskonen S, Hyyppä J, Vastaranta M (2022) Assessing the dependencies of Scots pine (*Pinus sylvestris* L.) structural characteristics and internal wood property variation. Forests 13(3):397. https://doi.org/10.3390/f13030397

Karjalainen V, Koivumäki N, Hakala T, George A, Muhojoki J, Hyyppa E, Suomalainen J, Honkavaara E (2024) Autonomous robotic drone system for mapping forest interiors. Int Arch Photogramm Remote Sens Spat Inf Sci 48(2):167–172. https://doi.org/10.5194/isprs-archives-XLVIII-2-2024-167-2024

Laasasenaho J (1982) Taper curve and volume functions for pine, spruce and birch. Communicationes Instituti forestalis Fenniae. The Finnish Forest Research Institute, 108, p. 1–74. https://helka.helsinki.fi/permalink/358UOH_INST/17sob7u/alma99611623506253

Lachenbruch B, Moore JR, Evans R (2011) Radial variation in wood structure and function in woody plants, and hypotheses for its occurrence. In: Size- and age-related changes in tree structure and function (pp. 121–164). Springer. https://doi.org/10.1007/978-94-007-1242-3_5

Lessard E, Fournier R, Luther J, Mazerolle M, Van Lier O (2014) Modeling wood fiber attributes using forest inventory and environmental data for Newfoundland's boreal forest. For Ecol Manage 313:307–318. https://doi.org/10.1016/j.foreco.2013.10.030

Liu C, Olson JR, Tian Y, Shen Q (1988) Theoretical wood densitometry: I mass attenuation equations and wood density models. Wood Fiber Sci 20(1):22–34

Longuetaud F, Mothe F, Leban JM (2007) Automatic detection of the heartwood/sapwood boundary within Norway spruce (*Picea abies* (L.) Karst.) logs by means of CT images. Comput Electron Agric 58(2):100–111. https://doi.org/10.1016/j.compag.2007.03.010

Luther JE, Skinner R, Fournier RA, van Lier OR, Bowers WW, Coté J-F, Hopkinson C, Moulton T (2014) Predicting wood quantity and quality attributes of balsam fir and black spruce using airborne laser scanner data. Forestry 87(2):313–326. https://doi.org/10.1093/forestry/cpt039

Mäkelä A, Grace J, Deckmyn G, Kantola A, Kint V (2010) Simulating wood quality in forest management models. For Syst 19(4):48–68. https://doi.org/10.5424/fs/201019S-9314

Mäkinen H, Ojansuu R, Sairanen P, Yli-Kojola H (2003) Predicting branch characteristics of Norway spruce (*Picea abies* (L.) Karst.) from simple stand and tree measurements. Forestry 76(5):525–546. https://doi.org/10.1093/forestry/76.5.525

Moberg L (2006) Predicting knot properties of *Picea abies* and *Pinus sylvestris* from generic tree descriptors. Scand J Forest Res 21:48–61. https://doi.org/10.1080/14004080500487011

Moore JR, Lyon AJ, Searles GJ, Vihermaa LE (2009) The effects of site and stand factors on the tree and wood quality of Sitka spruce growing in the United Kingdom. Silva Fenn 43(3):383–396. https://doi.org/10.14214/sf.195

Nocetti M, Brunetti M (2024) Advancements in wood quality assessment: standing tree visual evaluation—a review. Forests 15(6):943. https://doi.org/10.3390/f15060943

Oja J, Wallbäcks L, Grundberg S, Hägerdal E, Grönlund A (2003) Automatic grading of Scots pine (*Pinus sylvestris* L.) sawlogs using an industrial X-ray log scanner. Comput Electron Agric 41(1):63–75. https://doi.org/10.1016/S0168-1699(03)00042-5

Oja J, Grundberg S, Fredriksson J, Berg P (2004) Automatic grading of sawlogs: a comparison between X-ray scanning, optical three-dimensional scanning and combinations of both methods. Scand J Forest Res 19(1):89–95. https://doi.org/10.1080/02827580310019563

Olson JR, Liu C, Tian Y, Shen Q (1988) Theoretical wood densitometry: II. Optimal X-ray energy for wood density measurement. Wood Fiber Sci 20(2):187–196

Pinheiro JC, Bates DM (2009) Mixed-effects models in S and S-PLUS. Series: Statistics and Computing. Springer Science & Business Media. ISBN: 9781441903174

Pokharel B, Groot A, Pitt D, Woods M, Dech J (2016) Predictive modeling of black spruce (*Picea mariana* (Mill.) BSP) wood density using stand structure variables derived from airborne LiDAR data in boreal forests of Ontario. Forests 7(12):311. https://doi.org/10.3390/f7120311

Pretzsch H (2021) The social drift of trees. Consequence for growth trend detection, stand dynamics, and silviculture. Eur J Forest Res 140:703–719. https://doi.org/10.1007/s10342-020-01351-y

Puliti S, McLean JP, Cattaneo N, Fischer C, Astrup R (2023) Tree height-growth trajectory estimation using uni-temporal UAV laser scanning data and deep learning. Forestry Int J Forest Res 96(1):37–48. https://doi.org/10.1093/forestry/cpac026

Pyörälä J, Kankare V, Vastaranta M, Rikala J, Holopainen M, Sipi M, Hyyppä J, Uusitalo J (2018a) Comparison of terrestrial laser scanning and X-ray scanning in measuring Scots pine (*Pinus sylvestris* L.) branch structure. Scand J Forest Res 33(3):291–298. https://doi.org/10.1080/02827581.2017.1355409

Pyörälä J, Liang X, Saarinen N, Kankare V, Wang Y, Holopainen M, Hyyppä J, Vastaranta M (2018b) Assessing branching structure for biomass and wood quality estimation using terrestrial laser scanning point clouds. Can J Remote Sens 44(5):462–475. https://doi.org/10.1080/07038992.2018.1557040

Pyörälä J, Kankare V, Liang X, Saarinen N, Rikala J, Kivinen V-P, Sipi M, Holopainen M, Hyyppä J, Vastaranta M (2019a) Assessing log geometry and wood quality in standing timber using terrestrial laser-scanning point clouds. Forestry 92(2):177–187. https://doi.org/10.1093/forestry/cpy044

Pyörälä J, Saarinen N, Kankare V, Coops NC, Liang X, Wang Y, Holopainen M, Hyyppä J, Vastaranta M (2019b) Variability of wood properties using airborne and terrestrial laser scanning. Remote Sens Environ 235:111474. https://doi.org/10.1016/j.rse.2019.111474

Qi Y, Coops NC, Daniels LD, Butson CR (2022) Comparing tree attributes derived from quantitative structure models based on drone and mobile laser scanning point clouds across varying canopy cover conditions. ISPRS J Photogramm Remote Sens 192:49–65. https://doi.org/10.1016/j.isprsjprs.2022.07.021

R CT (2023) R: a language and environment for statistical computing. In (Version 4.3.0) R Foundation for Statistical Computing. https://www.R-project.org/

Rathgeber CB, Cuny HE, Fonti P (2016) Biological basis of tree-ring formation: a crash course. Front Plant Sci 7:734. https://doi.org/10.3389/fpls.2016.00734

Raumonen P, Kaasalainen M, Akerblom M, Kaasalainen S, Kaartinen H, Vastaranta M, Holopainen M, Disney M, Lewis P (2013) Fast automatic precision tree models from terrestrial laser scanner data. Remote Sens 5(2):491–520. https://doi.org/10.3390/rs5020491

Roussel JR, Auty D (2024) Airborne LiDAR data manipulation and visualization for forestry applications. In https://CRAN.R-project.org/package=lidR

Roussel J-R, Auty D, Coops NC, Tompalski P, Goodbody TRH, Meador AS, Bourdon J-F, de Boissieu F, Achim A (2020) LidR: an R package for analysis of Airborne Laser Scanning (ALS) data. Remote Sens Environ 251:112061. https://doi.org/10.1016/j.rse.2020.112061

Sagar A, Kärhä K, Einola K, Koivusalo A (2024) Assessing the potential of onboard LiDAR-based application to detect the quality of tree stems in cut-to-length (CTL) harvesting operations. Forests 15(5):818. https://doi.org/10.3390/f15050818

Saikkonen O, Pyörälä J, Luoma V, Valkonen S, Hyyppä J, Holopainen M (n.d.) (In review) Evaluation of generic stem taper function in continuous-cover Norway spruce forests. [Preprint]. https://doi.org/10.31219/osf.io/db8xj

Sandberg D, Fink G, Hasener J, Kairi M, Marhenke T, Ross RJ, Steiger R, Wang X (2023) Process control and grading in primary wood processing. In: Springer handbook of wood science and technology. Springer International Publishing, pp. 1019–1073. https://doi.org/10.1007/978-3-030-81315-4_20

van Ewijk KY, Treitz PM, Scott NA (2011) Characterizing forest succession in Central Ontario using LiDAR-derived indices. Photogramm Eng Remote Sens 77(3):261–269. https://doi.org/10.14358/PERS.77.3.261

Van Leeuwen M, Hilker T, Coops NC, Frazer G, Wulder MA, Newnham GJ, Culvenor DS (2011) Assessment of standing wood and fiber quality using ground and airborne laser scanning: a review. For Ecol Manage 261(9):1467–1478. https://doi.org/10.1016/j.foreco.2011.01.032

Vauhkonen J, Packalen T (2018) Uncertainties related to climate change and forest management with implications on climate regulation in Finland. Ecosyst Serv 33:213–224. https://doi.org/10.1016/j.ecoser.2018.02.011

Wang Y, Kukko A, Hyyppä E, Hakala T, Pyörälä J, Lehtomäki M, El Issaoui A, Yu X, Kaartinen H, Liang X (2021) Seamless integration of above-and under-canopy unmanned aerial vehicle laser scanning for forest investigation. For Ecosyst 8:10. https://doi.org/10.1186/s40663-021-00290-3

Wei Q, Leblon B, La Rocque A (2011) On the use of X-ray computed tomography for determining wood properties: a review. Can J for Res 41(11):2120–2140. https://doi.org/10.1139/X11-111

Winberg O, Pyörälä J, Yu X, Kaartinen H, Kukko A, Holopainen M, Holmgren J, Lehtomäki M, Hyyppä J (2023) Branch information extraction from Norway spruce using handheld laser scanning point clouds in Nordic forests. ISPRS Open Journal of Photogrammetry and Remote Sensing 9:100040. https://doi.org/10.1016/j.ophoto.2023.100040

Yrttimaa T, Kankare V, Luoma V, Junttila S, Saarinen N, Calders K, Holopainen M, Hyyppa J, Vastaranta M (2023) A method for identifying and segmenting branches of Scots pine (*Pinus sylvestris* L.) trees using terrestrial laser scanning. Forestry 97(4):531–545. https://doi.org/10.1093/forestry/cpad062

Zeller L, Pretzsch H (2019) Effect of forest structure on stand productivity in Central European forests depends on developmental stage and tree species diversity. For Ecol Manage 434:193–204. https://doi.org/10.1016/j.foreco.2018.12.024

Publisher's Note